

## Regular Article

# Facile Low-Temperature synthesis of novel carbon nitrides for efficient conversion of carbon dioxide into Value-Added chemicals

Hushan Chand<sup>a</sup>, Preeti Bhumla<sup>b,1</sup>, Subhadip Goswami<sup>a,1</sup>, Nicolò Allasia<sup>c</sup>, Gianvito Vilé<sup>c,\*</sup>, Saswata Bhattacharya<sup>b,\*</sup>, Venkata Krishnan<sup>a,\*</sup>

<sup>a</sup> School of Chemical Sciences and Advanced Materials Research Center, Indian Institute of Technology Mandi, Kamand, Mandi 175075, Himachal Pradesh, India

<sup>b</sup> Department of Physics, Indian Institute of Technology Delhi, New Delhi 110016, India

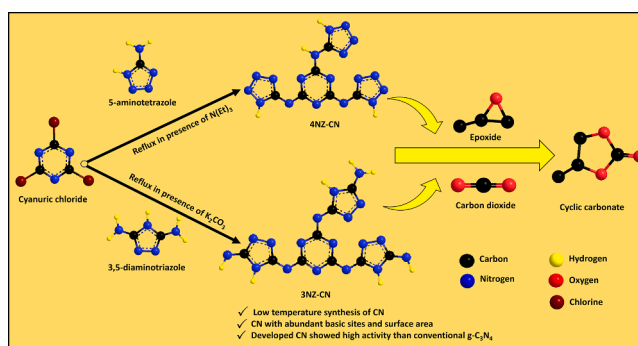
<sup>c</sup> Department of Chemistry, Materials, and Chemical Engineering "Giulio Natta", Polytechnics di Milano, Piazza Leonardo da Vinci 32, IT-20133 Milano, Italy



## HIGHLIGHTS

- Novel carbon nitride catalysts prepared with cost-effective, low-temperature methods.
- The materials show enhanced properties, higher surface areas and abundant basic sites.
- Their catalytic activity is superior to conventional carbon nitride.
- Threefold increase in CO<sub>2</sub> cycloaddition efficiency and stable catalytic activity.
- This advancement has potential for converting CO<sub>2</sub> into valuable chemicals.

## GRAPHICAL ABSTRACT



## ARTICLE INFO

## Keywords:

Low temperature synthesis  
Novel carbon nitride  
Economically viable synthesis  
CO<sub>2</sub> conversion  
Kinetic studies

## ABSTRACT

The interest in using carbon nitrides (CN) for CO<sub>2</sub> conversion has stimulated extensive research on CN synthesis. Herein, we report the synthesis of two novel CN materials using low-cost commercially available precursors at low temperatures in a short duration of time. Two CN materials, one derived from 5-amino tetrazole (named 4NZ-CN) and the other derived from 3, 5-diamino-1, 2, 4-triazole (named 3NZ-CN) precursors, are prepared by refluxing these precursors for 2 h at 100 °C. 4NZ-CN and 3NZ-CN catalysts show higher surface areas (55.80 and 52.00 m<sup>2</sup> g<sup>-1</sup>) and more basic sites (10.05 and 5.65 mmol g<sup>-1</sup>) than the conventional graphitic carbon nitride (g-C<sub>3</sub>N<sub>4</sub>) derived from melamine, for which the corresponding values are 9.20 m<sup>2</sup> g<sup>-1</sup> and 0.62 mmol g<sup>-1</sup>, respectively. In addition, both CN exhibit a 3-fold higher catalytic activity for CO<sub>2</sub> cycloaddition to epoxides than g-C<sub>3</sub>N<sub>4</sub>. The structure–activity relationship was ascertained using a combination of experimental and computational studies, and a catalytic mechanism was proposed. This work provides a facile strategy for the synthesis of novel CN materials at relatively low temperatures, and the developed catalysts show remarkable performance in the conversion of CO<sub>2</sub> to value-added chemicals.

\* Corresponding authors.

E-mail addresses: [gianvito.vile@polimi.it](mailto:gianvito.vile@polimi.it) (G. Vilé), [saswata@physics.iitd.ac.in](mailto:saswata@physics.iitd.ac.in) (S. Bhattacharya), [vkn@iitmandi.ac.in](mailto:vkn@iitmandi.ac.in) (V. Krishnan).

<sup>1</sup> These authors contributed equally to this work.

<https://doi.org/10.1016/j.jcis.2024.06.031>

Received 5 March 2024; Received in revised form 27 May 2024; Accepted 4 June 2024

Available online 6 June 2024

0021-9797/© 2024 Elsevier Inc. All rights are reserved, including those for text and data mining, AI training, and similar technologies.

## 1. Introduction

Due to the escalating environmental deterioration caused by anthropogenic CO<sub>2</sub> emissions, the global community is committed to reducing carbon footprints and combatting climate change [1,2]. Consequently, scientists are striving to develop environmentally benign technologies that can meet the world's energy demand while minimizing carbon footprint [3]. The conversion of CO<sub>2</sub> into valuable chemicals represents a viable pathway towards CO<sub>2</sub> mitigation and must be explored to its full potential to achieve a carbon-neutral energy cycle [4–6]. Among the various strategies, CO<sub>2</sub> cycloaddition to cyclic carbonate has emerged as a promising approach due to the widespread use of cyclic carbonates in various applications, ranging from fine chemicals and pharmaceutical intermediates to synthetic fuels [7,8]. This reaction, however, is energy-intensive due to the chemical inertness of CO<sub>2</sub> [9]. One of the practical approaches to overcome this challenge is through the employment of catalysts that can lower the energy barrier of this process. Significant progress has been made in developing heterogeneous catalysts, and among them, carbon nitrides (CN) have found their place in catalyzing this reaction [10].

There is a growing research interest in CN-based materials for CO<sub>2</sub> cycloaddition to epoxides [4]. The major hurdle in this cycloaddition reaction is the activation of thermodynamically inert CO<sub>2</sub> molecules [11]. CN are well-known for their ability to activate CO<sub>2</sub> through acid-base interactions between the basic N sites of CN and the acidic C sites of CO<sub>2</sub> [12]. Additionally, the porosity, and the surface area of CN play a crucial role in facilitating this reaction more readily [13]. However, the simple CN explored so far for this cycloaddition reaction has shown less efficacy, which could be attributed to low N content and surface area [14,15]. Moreover, these reactions are performed under harsh conditions of high temperature and pressure, making this process highly energy-demanding [16]. Considering the low activity of CN for this reaction, it is highly desirable to synthesize CN with higher N content, increased surface area and sufficient porosity. CN exhibits tunable surface area, high porosity, presence of a plethora of basic nitrogen sites, nonmetallic semiconducting character, high chemical and thermal stability, and photochemical properties [17]. Generally, CN scaffolds are composed of sp<sup>2</sup> hybridized carbon and nitrogen atoms arranged in triazine or heptazine repeating units [18]. In this form, CN has been extensively employed for various applications [19]. However, most of the reported CN materials have been synthesized via thermal pyrolysis of different N-rich precursors (e.g., dicyandiamide, melamine, urea, etc.) using high-temperature conditions, rendering this process energy-intensive, environmentally unsustainable and resulting in low yields [20].

Current research interests in CN have been focused on its structural modification through adopting new synthesis routes, new precursors or inserting heteroatoms [4,21–23]. Recently, N-rich CN have garnered significant attention due to its ability to narrow down the band gap and increase CO<sub>2</sub> adsorption efficiency [4]. Vinu et al. pioneered work in this direction, preparing C<sub>3</sub>N<sub>4</sub>, C<sub>3</sub>N<sub>5</sub>, C<sub>3</sub>N<sub>6</sub> and C<sub>3</sub>N<sub>7</sub> based CN using 3-amino-1,2,4-triazine, 3-amino-1,2,4-triazole and 5-aminotetrazole precursors [4,24]. Recently, the same authors have prepared sulfur-doped C<sub>3</sub>N<sub>5</sub> using 5-amino-1,3,4-thiadiazole-2-thiol and its structure contains one triazole and two triazine motifs with trivial ratios of thiadiazole on the edges [25]. In another work, Shankar et al. prepared C<sub>3</sub>N<sub>5</sub> by thermal deammoniation of the melem hydrazine precursor, wherein two heptazine units are linked through an azo linkage [26]. In all these works, CNs were produced through high-temperature treatments. The need for high temperature resulted in the CN having a disordered CN framework and a lower nitrogen content. Further, the yield of CN obtained from the synthesis was lower than the amount of precursor used initially [27]. Therefore, there is an urgent need to come up with an alternate environmentally benign synthesis approach that enables the high-yield CN synthesis at relatively lower temperatures.

In this work, we report a new synthesis approach for producing CN

materials with higher surface area, abundant N content and structural alterations. In particular, we have synthesized two CN materials: one by polymerization of 5-aminotetrazole (4NZ) and cyanuric chloride and another by polymerization of 3, 5-diamino-1, 2, 4-triazole (3NZ) and cyanuric chloride. Both these materials were prepared at 100 °C within a short period of 2 h. The approach is facile, scalable, and economically favorable, as it uses a very simple reaction setup, mild reaction conditions, and cheap, readily available synthesis precursors. Further, this process is less energy-intensive and environmentally sustainable as it offers the use of very low reaction temperatures and short reaction times, contrary to previously reported methods for conventional CN synthesis. The structural and compositional studies revealed that both 4NZ-CN and 3NZ-CN resemble typical melamine-derived graphitic carbon nitride (g-C<sub>3</sub>N<sub>4</sub>) in various aspects. The optical properties of 4NZ-CN and 3NZ-CN are similar to those of conventional g-C<sub>3</sub>N<sub>4</sub>. Textural studies revealed that both 4NZ-CN and 3NZ-CN possess a mesoporous nature with a higher surface area than g-C<sub>3</sub>N<sub>4</sub>. Temperature programmed desorption (TPD) studies revealed an increased number of basic sites in 4NZ-CN and 3NZ-CN compared to g-C<sub>3</sub>N<sub>4</sub>, attributed to their abundant N content. The catalytic activity of 4NZ-CN and 3NZ-CN was tested for CO<sub>2</sub> cycloaddition to epoxides under solvent-free and mild conditions of temperature and atmospheric pressure. The materials demonstrated remarkable catalytic activity compared to g-C<sub>3</sub>N<sub>4</sub>. The catalysts have shown wide applicability to various other substrates, giving good to excellent conversion to their corresponding products. Additionally, kinetic and thermodynamic studies indicate that the reaction follows first-order kinetics, with a significant lowering of the reaction energy barrier when mediated by these materials as catalysts.

## 2. Materials and methods

### 2.1. Synthesis of 5-aminotetrazole-derived carbon nitride (4NZ-CN)

4NZ-CN was synthesized by adding 2.1 mmol of 5-aminotetrazole (4NZ) in a round bottom flask containing 7 mL of 1,4-dioxane solvent. To this mixture, 2.1 mmol of triethylamine was added and stirred for 30 min at room temperature (RT). Simultaneously, in a separate beaker, 0.7 mmol of cyanuric chloride was dissolved in 7 mL of 1,4-dioxane, and the solution was well shaken to ensure the complete solubilization of cyanuric chloride. This solution was then added to the 5-aminotetrazole solution, and the reaction was refluxed at 100 °C under N<sub>2</sub> for 2 h. Upon reaction completion, the product was collected by filtration and washed with 1,4-dioxane (3 times), deionized water (3 times), and ethanol (2 times). Finally, yellow powdered 4NZ-CN was obtained after drying in an oven at 80 °C for 24 h (optical image given in Fig. S1a) and used for further characterization.

### 2.2. Synthesis of 3, 5-diamino-1, 2, 4-triazole derived carbon nitride (3NZ-CN)

The procedure adopted for 3NZ-CN synthesis was almost similar to that of 4NZ-CN, with some minor modifications. Here, we have used K<sub>2</sub>CO<sub>3</sub> as a base in place of triethylamine. In brief, 0.40 mmol of 3, 5-diamino-1, 2, 4-triazole (3NZ) was poured into a round bottom flask, enclosing 6 mL of 1,4-dioxane solvent. To this solution, 0.80 mmol of K<sub>2</sub>CO<sub>3</sub> was added, and the mixture was stirred for 30 min at RT. Then, 0.27 mmol of cyanuric chloride was introduced in a separate beaker containing 6 mL of 1,4-dioxane, and the solution was thoroughly shaken to ensure the complete solubilization of cyanuric chloride. This solution was added to 3, 5-diamino-1, 2, 4-triazole solution, which was then refluxed at 100 °C under N<sub>2</sub> for 2 h. Upon reaction completion, the product was collected by filtration and washed with 1,4-dioxane (3 times), deionized water (3 times), and ethanol (2 times). Finally, a pale-yellow powder of 3NZ-CN was obtained after drying in an oven at 80 °C for 24 h (optical image given in Fig. S1b) and used for further characterization.

### 2.3. Synthesis of graphitic carbon nitride (g-C<sub>3</sub>N<sub>4</sub>)

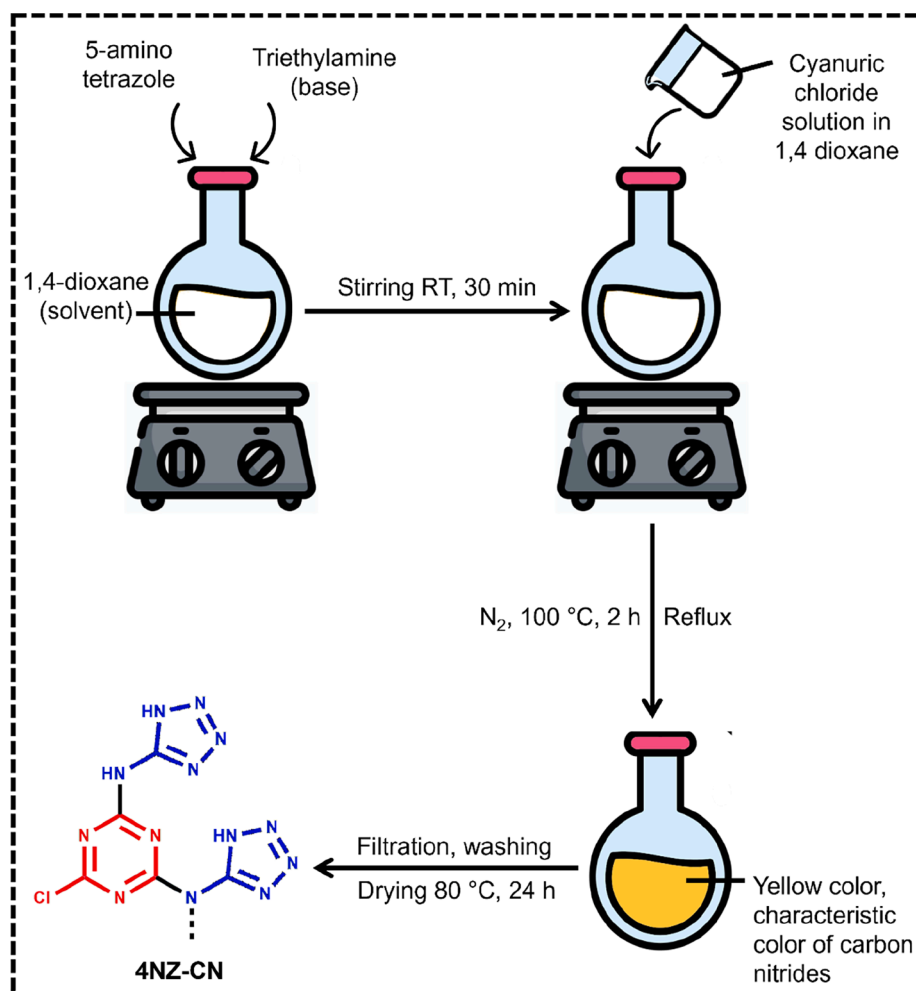
The conventional graphitic carbon nitride (g-C<sub>3</sub>N<sub>4</sub>) was prepared using melamine precursor through the thermal calcination method, as reported in the literature [12]. In particular, 5 g of melamine was poured into alumina crucibles and calcinated at 450 °C for 3 h with a ramp rate of 5 °C min<sup>-1</sup>. The resulting, yellow-colored bulk g-C<sub>3</sub>N<sub>4</sub> was then pulverized to a fine powder by using a mortar and pestle and further exfoliated at 500 °C for 2 h at a ramp rate of 5 °C min<sup>-1</sup> to obtain the g-C<sub>3</sub>N<sub>4</sub> nanosheets.

### 2.4. Catalytic cycloaddition of CO<sub>2</sub> to epoxides

For a typical reaction, a particular mass of catalyst (30 mg in the case of 4NZ-CN and 50 mg in the case of 3NZ-CN) and 20 mg of KI were weighed and added in a round bottom flask. Subsequently, 20 mmol epichlorohydrin was poured inside, and the flask was sealed with a condenser. The vessel was connected to a suction pump to evacuate the air. Afterward, a CO<sub>2</sub> balloon was attached to the condenser. The reactions were performed at 100 °C for 24 h without any solvent. Upon reaction completion, the catalyst was recovered through filtration once the reaction vessel had cooled down to RT. Pure products were isolated through column chromatography, and their successful formation was examined using nuclear magnetic resonance (NMR) spectroscopy (sections S6 and S7).

### 2.5. Computational details

The spin-polarized density functional theory (DFT) calculations were performed using the plane-wave-based pseudopotential approach as implemented in the Vienna *ab initio* Simulation Package (VASP) [28]. The electron–ion interactions in all elemental constituents were described using the projector augmented wave (PAW) method [29]. To optimize the structures, the generalized gradient approximation expressed by the Perdew–Burke–Ernzerhof (PBE) exchange–correlation ( $\epsilon_{xc}$ ) functional was employed [30]. The structures were relaxed until the Heymann–Feynman forces acting on each atom were less than 0.001 eV Å<sup>-1</sup> utilizing the conjugate gradient minimization method. The Brillouin zone was sampled at the  $\Gamma$  point for all DFT calculations. For precise calculations, the electron wave function was expanded with an energy cutoff of 500 eV. The self-consistency loop was converged to a total energy threshold of 0.01 meV. The single-point energy calculations were carried out using HSE06  $\epsilon_{xc}$  functional [31,32]. A vacuum thickness of 15 Å was used to prevent the interactions between the periodic images. The minimum energy path was calculated using the climbing-image nudged elastic band (CI-NEB) method [33]. The two-body vdW interaction as devised by Tkatchenko–Scheffler has been employed [34]. All structures were visualized using the Visualization for Electronic and Structural Analysis (VESTA) software [35].



Scheme 1. Schematic representation showing the synthesis of 4NZ-CN.

### 3. Results and discussion

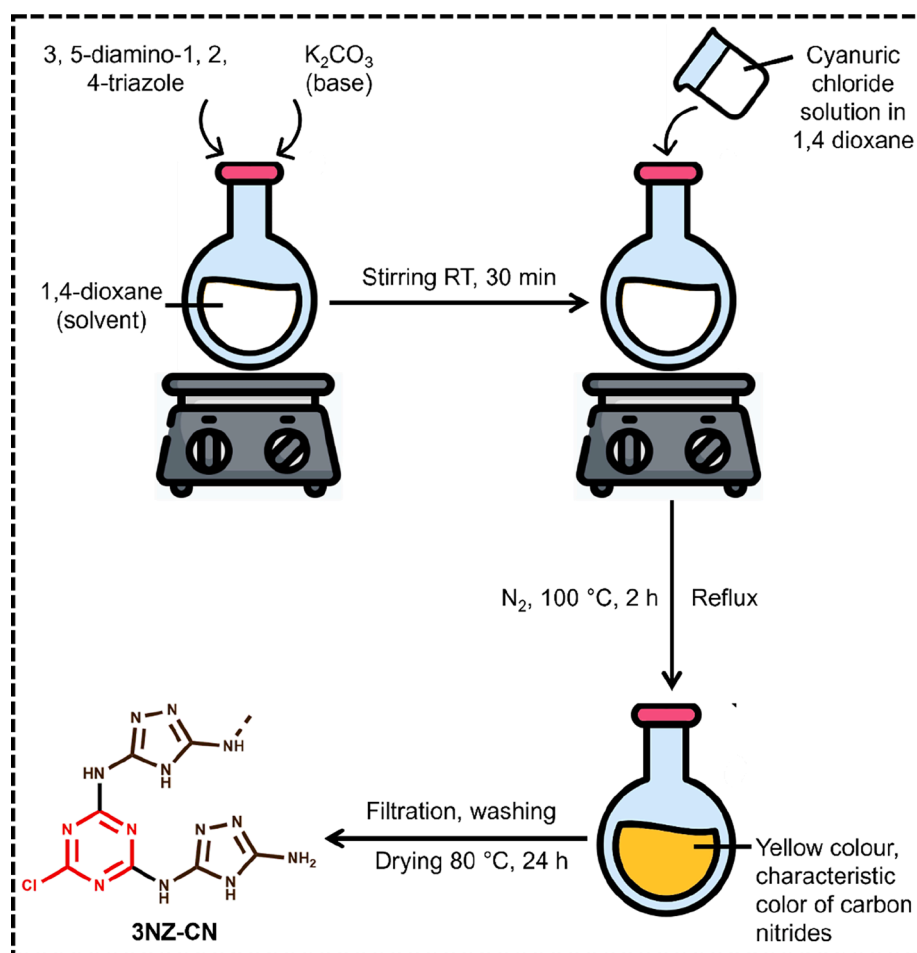
#### 3.1. Synthesis and structural studies

A new, facile, and sustainable approach was used to synthesize 4NZ-CN and 3NZ-CN through the polymerization of 5-aminotriazole and 3, 5-diamino-1, 2, 4-triazole precursors. These were mixed with cyanuric chloride in the presence of a suitable base (triethylamine in case of 4NZ-CN, and  $K_2CO_3$  for 3NZ-CN). A representative sketch for the synthesis of 4NZ-CN and 3NZ-CN is shown in Scheme 1 and 2, respectively. The color of the obtained 4NZ-CN and 3NZ-CN sample was yellow, which is characteristic of conventional carbon nitride materials. To confirm the successful synthesis, a battery of characterization methods was applied to determine the characteristics of the materials. Fig. 1a depicts the X-ray diffraction (XRD) patterns of  $g-C_3N_4$ , 4NZ-CN and 3NZ-CN. The first, related to  $g-C_3N_4$ , contains two characteristic peaks at  $2\theta$  values of  $13.2^\circ$  and  $27.1^\circ$ , indexed to (100) and (002), respectively [26]. The (100) peak corresponds to the interplanar arrangement of heptazine units, while the (002) peak is indexed to the interplanar stacking of repeating units in carbon nitride structure. The d-spacing corresponding to (100) plane was 0.67 nm, and 0.329 nm for (002) plane. Like  $g-C_3N_4$ , both 4NZ-CN and 3NZ-CN contain (002) peaks, located at  $27.3^\circ$  and  $26.9^\circ$   $2\theta$  values, respectively. The d-spacing values for (002) plane of 4NZ-CN and 3NZ-CN are 0.326 nm and 0.331 nm, respectively. However, unlike  $g-C_3N_4$ , (100) peak is missing in 4NZ-CN and 3NZ-CN, since they both do not contain a heptazine unit in their structures, rather it is triazine that is present within them [36]. Also, the XRD pattern of 3NZ-CN contains additional peaks at  $12.0^\circ$ ,  $17.0^\circ$ ,  $24.1^\circ$  and  $40.5^\circ$ , which may be attributed to the

potassium oxide impurities, used as a base during the synthesis of this material [37,38]. Additionally, the XRD pattern of 4NZ-CN and 3NZ-CN was also compared with their precursors (Fig. S2a, b), confirming the absence of signals deriving from the precursors, demonstrating in this way the successful synthesis of these carbon nitrides.

Fourier transform infrared (FTIR) spectra of 4NZ-CN and 3NZ-CN (Fig. 1b) exhibited features that are similar to  $g-C_3N_4$ . In all the samples, a broad region between  $2400\text{--}3650\text{ cm}^{-1}$  (highlighted with a red square) could be ascribed to  $-\text{OH}$  groups (due to the presence of water molecules adsorbed on the surface of the catalysts), and also residual  $-\text{NH}$  as well as  $\text{NH}_2$  groups coming from the synthesis [39]. The interval of frequencies between  $1100\text{--}1800\text{ cm}^{-1}$  (highlighted in blue) contains infrared signals that are assigned to the stretching vibrations of  $\text{C}-\text{N}$  and  $\text{C}=\text{N}$  bonds, together with bending modes of amino groups included in the heterocyclic skeletons of  $g-C_3N_4$ , 4NZ-CN and 3NZ-CN [40,41]. The multiple peaks between  $780\text{--}630\text{ cm}^{-1}$  (highlighted with a magenta square) in all the samples can be easily attributed to out-of-plane  $\text{N}-\text{H}$  bending vibrations [27]. A distinct band corresponding to breathing mode of  $g-C_3N_4$ , 4NZ-CN and 3NZ-CN heterocycles (highlighted in green) is observed at  $809$ ,  $806$  and  $800\text{ cm}^{-1}$ , respectively. Besides, there are a few additional IR bands in 4NZ-CN and 3NZ-CN spectra, indicating that their core structure differs from  $g-C_3N_4$ . The band related to the breathing mode of the  $g-C_3N_4$  structure at  $809\text{ cm}^{-1}$  is higher in intensity and sharper with respect to the corresponding signal in 4NZ-CN and 3NZ-CN, which indicates that the core structure of 4NZ-CN and 3NZ-CN is different (triazine based) from that of  $g-C_3N_4$  (heptazine based) [42].

Further, the emergence of a new peak around  $1425\text{ cm}^{-1}$  (highlighted with a violet square) in both 4NZ-CN and 3NZ-CN is assigned to



Scheme 2. Schematic representation showing the synthesis of 3NZ-CN.



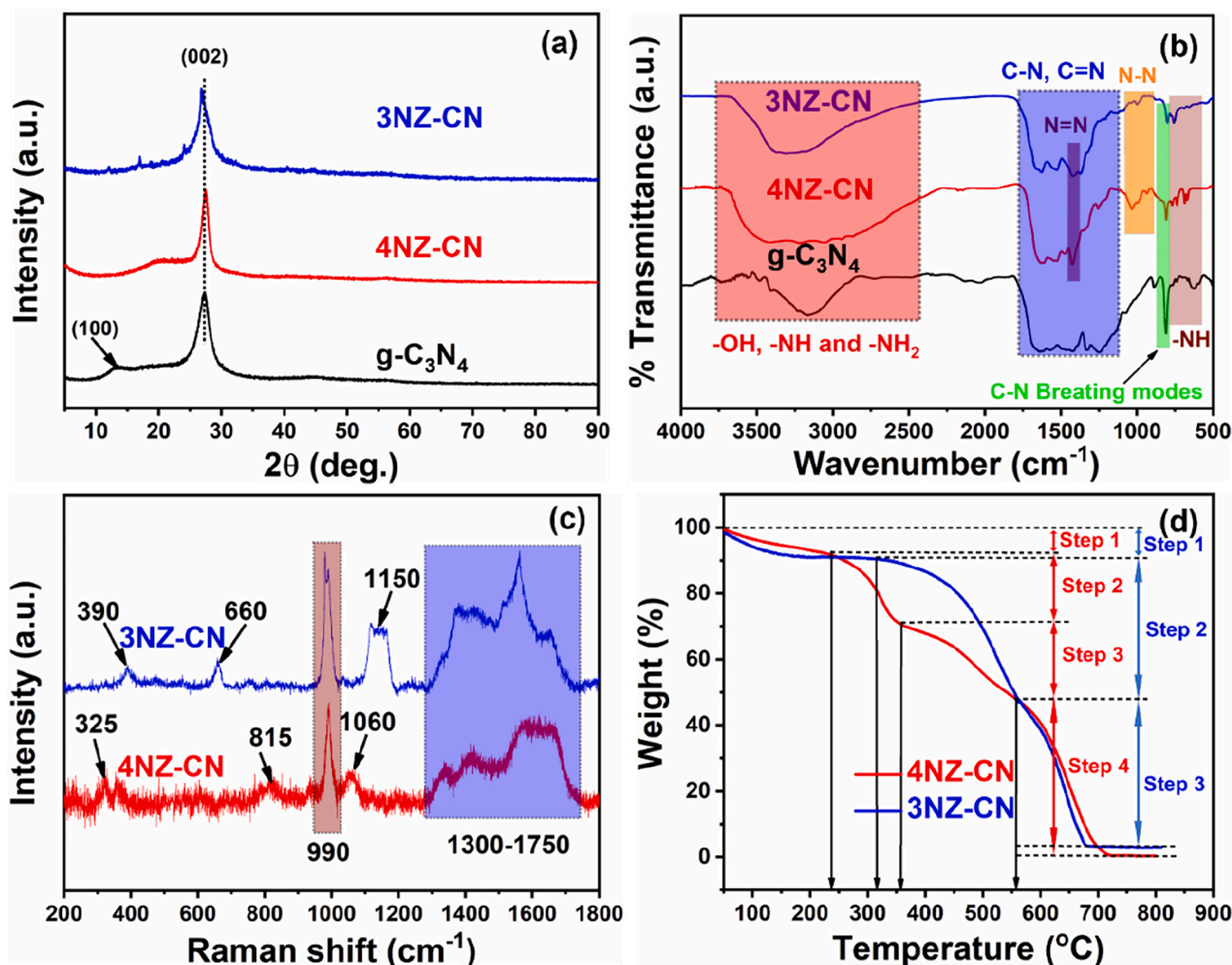


Fig. 1. (a, b) XRD patterns and FTIR spectra of  $g-C_3N_4$ , 4NZ-CN and 3NZ-CN, (c, d) Raman spectra and TGA plots of 4NZ-CN and 3NZ-CN.

the N=N bond, vindicating the presence of triazole and tetrazole units in 4NZ-CN and 3NZ-CN, respectively [43,44]. Moreover, this peak is notably stronger in intensity in 4NZ-CN than in 3NZ-CN due to more number of N=N bonds. In 4NZ-CN two peaks appear at 934 and 1032  $cm^{-1}$  (orange square) and could be assigned to antisymmetric wagging vibrations of amino groups and N—N stretching vibrations, respectively [45,46]. In 3NZ-CN the N—N stretching peak is observed at lower frequencies around 1000  $cm^{-1}$ . The weaker intensity of this signal in 3NZ-CN than in 4NZ-CN is again in accordance with the expectation, as it contains fewer N—N bonds. FTIR spectra of precursors and their corresponding products, such as 4NZ along with 4NZ-CN and cyanuric chloride, and 3NZ along with 3NZ-CN and cyanuric were also measured, as observable in Fig. S3a, b, which shows how the structure of 4NZ-CN and 3NZ-CN differs from their precursors. From Fig. S3a it is clear that the peaks corresponding to -NH (magenta highlighted) and N—N (highlighted in orange) functionalities in 4NZ, are also observed in 4NZ-CN with a slight shift. A sharp peak for breathing mode of triazine ring (represented with a black dotted line) in cyanuric chloride, is also present in 4NZ-CN. The existence of these peaks in 4NZ-CN reveals that its core structure contains triazine and tetrazole units. Similarly, 3NZ-CN (Fig. S3b) also shows the existence of these signals revealing the presence of triazine and triazole units in its core structure.

Raman spectra of 4NZ-CN and 3NZ-CN were acquired using 633 and 532 nm lasers, respectively, and are shown in Fig. 1c. The peaks observed around 1338 and 1600  $cm^{-1}$  in 4NZ-CN are attributed to D and G bands of graphene-type structure [47]. Similar D and G bands in 3NZ-CN are appeared around 1375 and 1560  $cm^{-1}$ , respectively. A broad

peak in both the samples ranging from 1300-1750  $cm^{-1}$  is assigned to  $sp^2$  and  $sp^3$  hybridized carbon atoms [48]. A sharp peak around 990  $cm^{-1}$  in both the samples is assigned to in-plane vibration of C—N bonds [49]. The signal around 325 and 815  $cm^{-1}$  in 4NZ-CN and 390 and 660  $cm^{-1}$  in 3NZ-CN can be assigned to breathing mode of triazine ring in their structures [26,50]. The signals located at around 1060 and 1150  $cm^{-1}$  in 4NZ-CN and 3NZ-CN, respectively, are assigned to N=N and C=N bonds, respectively [26,51]. Therefore, the Raman results complement FTIR studies. Thermogravimetric analysis (TGA) studies (Fig. 1d) were employed to assess the thermal stability of 4NZ-CN and 3NZ-CN. The TGA thermogram for both the materials shows four and three weight loss regimes, respectively, in temperature range of 25 to 900  $^{\circ}C$ . The first weight loss regime for 4NZ-CN and 3NZ-CN lies between 50–240 and 50–320  $^{\circ}C$ , respectively, and can be caused by the desorption of water molecules previously adsorbed on their surface [12]. The second, third and fourth regime for 4NZ-CN are found between 240–360, 360–560 and 560–720  $^{\circ}C$  and can be correlated to loss of triethylamine tethered to 4NZ-CN surface, loss of NH<sub>2</sub> groups, and condensation and degradation of 4NZ-CN heterocyclic structure, respectively [52]. In case of 3NZ-CN, the second and third regimes lie between 315–560 and 560–680  $^{\circ}C$ , respectively, and can be assigned to loss of NH<sub>2</sub> groups and condensation or degradation of 3NZ-CN heterocyclic structure, respectively. An extra weight loss regime between 240–360  $^{\circ}C$  observed in 4NZ-CN is ascribed to a loss of triethylamine tethered to 4NZ-CN, tethered to its structure. This regime is missing in 3NZ-CN, which is expected, since for the production of 3NZ-CN,  $K_2CO_3$  was used in the place of triethylamine. In addition, 4NZ-CN is thermally

less stable than 3NZ-CN, which is likely due to presence of higher thermally unstable N–N bonds in 4NZ-CN [53].

More detailed structural insights of 4NZ-CN and 3NZ-CN were investigated using Solid-State Cross-Polarization Magic-Angle Spinning Nuclear Magnetic Resonance (CP-MAS NMR) spectroscopic technique. Before performing these measurements, liquid-state NMR spectra of precursors, i.e., 5-aminotetrazole, 3, 5-diamino-1, 2, 4-triazole and cyanuric chloride were acquired, with the aim of helping in the evaluation of the solid-state NMR spectra of 4NZ-CN and 3NZ-CN.  $^1\text{H}$  NMR spectrum of 5-aminotetrazole (Fig. S4) exhibits two peaks at 14.3 and 6.4 ppm, assigned to two types of hydrogen atoms that differ in terms of bonds and chemical environment: one is bonded to nitrogen in the ring of the compound, the other belongs to the free amino group attached to the core tetrazole structure. The  $^{13}\text{C}$  NMR spectrum (Fig. S5) shows a single peak at 156.9 ppm, easily assignable to the only carbon atom that is part of the tetrazole ring [54]. The  $^1\text{H}$  NMR spectrum of 3, 5-diamino-1, 2, 4-triazole (Fig. S6) contains two signals at 10.7 and 5.1 ppm, ascribed to two types of hydrogens, one bonded to a nitrogen atom within the triazole ring and the other one to the free amino groups. On the other hand, its  $^{13}\text{C}$  NMR spectrum (Fig. S7) displays a clear signal at 158.8 ppm, whose presence is related to the carbon atoms that are part of the triazole ring [55]. The  $^{13}\text{C}$  NMR spectrum (Fig. S8) of cyanuric chloride contains one peak at 149.8 ppm, which is likely attributable to the equivalent carbon atoms within the heterocyclic ring of this compound [56].

The  $^1\text{H}$  CP-MAS NMR spectrum of 4NZ-CN (Fig. 2a) shows five main signals localized at 14.5, 11.8, 6.3, 4.0 and 1.9 ppm. The two peaks at 14.5 and 6.3 ppm may be ascribed to the same features as in the CP-MAS NMR spectra of the tetrazole precursor, but with a slight change in chemical shift values. The presence of the 6.3 ppm peak indicates that

not all the hydrogen atoms bonded to bridging nitrogen atoms are used for chain propagation, and some remain after the reaction. The other three signals at 11.8, 4.0 and 1.9 ppm are assigned to protons belonging to impurities, possibly triethylamine hydrochloride [57], formed due to reaction between triethylamine (used as a base) and chloride of cyanuric chloride. In the  $^{13}\text{C}$  CP-MAS NMR spectrum of 4NZ-CN (Fig. 2b), three evident signals are localized at 162.1, 157.0 and 150.2 ppm, deriving from the presence of carbons that are part of the tetrazole and of triazine ring, of which they resemble closely with their chemical shifts. In particular, the first two may be related to carbon atoms bonded to bridging –NH and free amino groups, whose existence is due to a non-complete polymerization during the synthesis of 4NZ-CN. The third signal at 150.2 ppm likely originates from carbon atoms in the triazine ring of 4NZ-CN. Two additional signals positioned at 43.7 and 13.2 ppm are likely due to the presence of carbon atoms within the structure of the already mentioned triethylamine hydrochloride impurity [58].

Based on the previous CP-MAS NMR measurements, the proposed structure of 4NZ-CN is shown in Fig. S9 together with the polymerization mechanism. It contains tetrazole and triazine rings connected through nitrogen atoms that were formerly part of the free amino groups of the tetrazole precursor. In the first step, the formation of an amino anion occurs upon proton abstraction, operated by triethylamine, from the amino group of 5-amino tetrazole. The amino anion replaces chloride atoms of cyanuric acid via nucleophilic substitution, forming a 4NZ-CN monomer. The bridging –NH group is then used for the chain propagation, leading to the formation of the final polymer 4NZ-CN. From solid-state NMR results, it can also be also deduced that not all the hydrogen atoms of –NH bridging groups are used for the chain propagation, since some remain unpolymerized, fact that is for instance demonstrated by the presence of a peak at 6.3 ppm in the  $^1\text{H}$  CPMAS

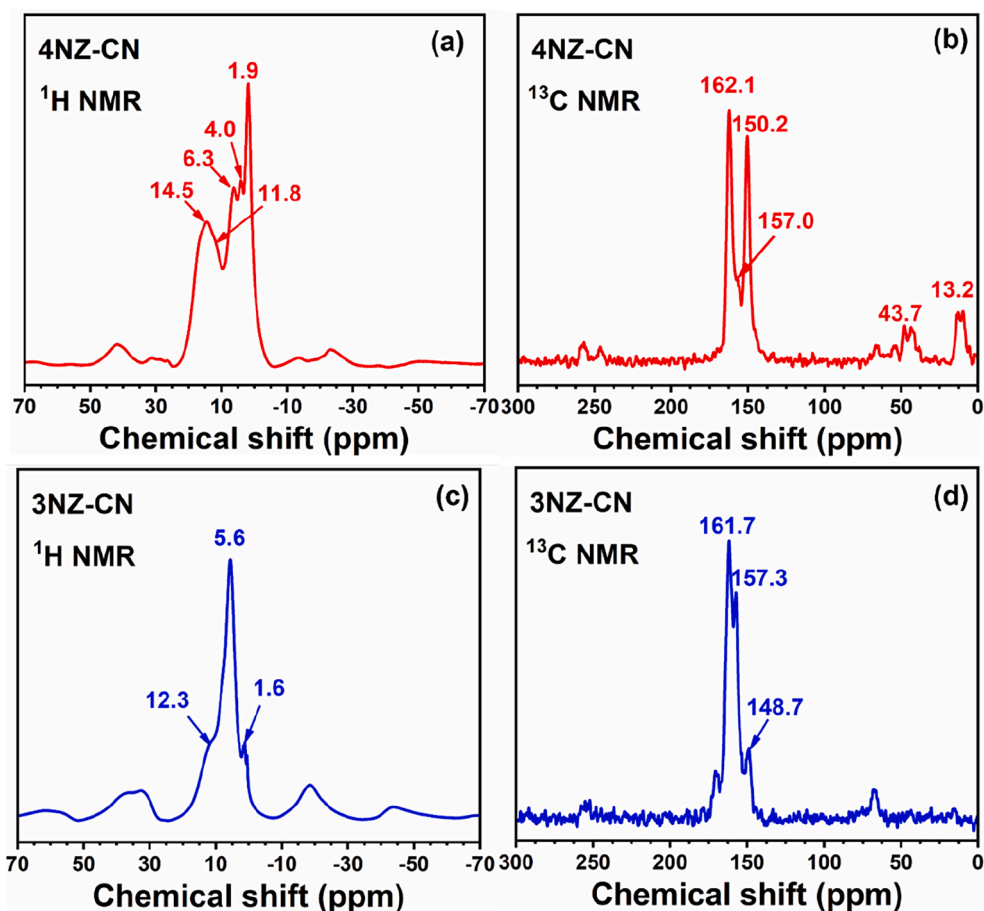


Fig. 2. CPMAS NMR spectra (a)  $^1\text{H}$  of 4NZ-CN, (b)  $^{13}\text{C}$  of 4NZ-CN, (c)  $^1\text{H}$  of 3NZ-CN and (d)  $^{13}\text{C}$  of 3NZ-CN.

spectra of 4NZ-CN. The  $^1\text{H}$  CP-MAS NMR spectrum of 3NZ-CN (Fig. 2c) shows a specific signal at 12.3, ppm, assignable to hydrogen atoms bonded to one of the nitrogen atoms composing the triazole ring structure of the precursor. Two additional peaks at 5.6 and 1.6 ppm may be related to the presence of hydrogen bonded to bridging nitrogen atoms and to free  $-\text{NH}_2$  groups that remain unpolymerized after the reaction synthesis. The  $^{13}\text{C}$  CP-MAS NMR spectrum of 3NZ-CN (Fig. 2d) displays three main signals at 161.7, 157.3 and 148.7 ppm. The first two may be supposedly assigned to carbons bonded to bridging  $-\text{NH}$  groups and to free amino groups that did not participate in the polymerization process of the catalyst. The third signal at 148.7 ppm is probably related to the presence of carbon atoms in the triazine ring of 3NZ-CN. The existence of additional signals in  $^1\text{H}$  CP-MAS NMR and  $^{13}\text{C}$  CP-MAS spectra is a clear index of the existence of some amino groups that remain unpolymerized after the reaction of synthesis of 3NZ-CN. In accordance with CP-MAS NMR data, the chemical structure of 3NZ-CN is shown in Fig. S10. It is chemically composed of triazole and triazine rings, connected through nitrogen atoms that were previously part of the free  $-\text{NH}_2$  groups

belonging to the triazole precursor. Initially, the production of an amino anion takes place through a proton abstraction, performed by  $\text{K}_2\text{CO}_3$ , from amino groups of 3, 5-diamino-1, 2, 4-triazole. This step is followed by a nucleophilic substitution of the anion on the cyanuric acid, with the final formation of a 3NZ-CN monomer. Differently from 4NZ-CN, in 3NZ-CN the free  $-\text{NH}_2$  substituents of the triazole precursor are the ones used in the chain propagation process, rather than the bridging  $-\text{NH}$  groups. The presence of some unpolymerized amino groups in both 3NZ-CN and 3NZ-CN reveal that these catalysts undergo an incomplete polymerization during their synthesis, unlike  $\text{g-C}_3\text{N}_4$ .

### 3.2. Morphological and compositional studies

Morphological aspects were studied using scanning electron microscopy (SEM) and transmission electron microscopy (TEM). Fig. 3a depicts the SEM images of 4NZ-CN, revealing the sheet-like morphology of this sample. Fig. 3b, c presents the TEM and HRTEM images, that also confirms the SEM results, depicting the sheet-like architecture of 4NZ-

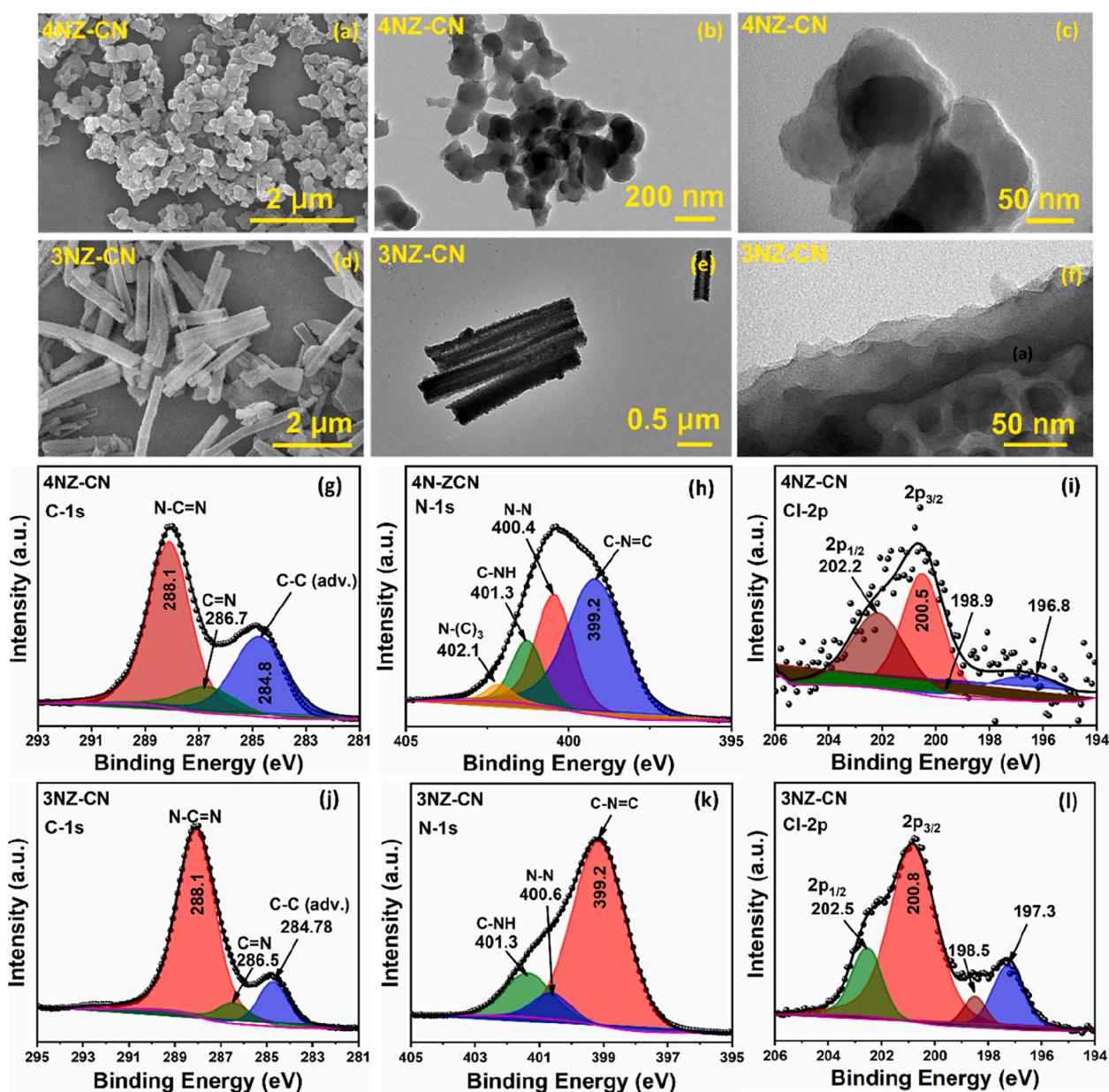


Fig. 3. (a-c) and (d-f) are SEM and TEM images of 4NZ-CN and 3NZ-CN, respectively, (g-i) and (j-l) high resolution XPS spectra of C-1 s, N-1 s and Cl-2p in 4NZ-CN and 3NZ-CN, respectively.



CN. Fig. 3d and e, f presents the SEM, TEM and HRTEM images of 3NZ-CN which possess nanotube-like tridimensional structure. The energy dispersive X-ray (EDX) spectra (Fig. S11) shows the predominant presence of C and N, along with a small amount of O arising from atmospheric oxygen or due to sample preparation in ethanol solvent. Additionally, a prominent peak around 1.72 KeV is attributed to Si, which originates due to use of silicon wafers during the SEM measurements. X-ray photoelectron spectroscopy (XPS) was used to investigate the valence states and bonding features of 4NZ-CN and 3NZ-CN. Fig. S12 depicts the XPS survey spectrum of 4NZ-CN and 3NZ-CN. The atomic percentage of different elements in g-C<sub>3</sub>N<sub>4</sub>, 4NZ-CN and 3NZ-CN along with N/C ratio is tabulated in Table S1. Both 4NZ-CN and 3NZ-CN contain C and N as major constituents with a small amount of O attributed to atmospheric oxygen adsorbed on the catalysts surface. The atomic percentages of C and N in 4NZ-CN are 38.50% and 55.99%, respectively, while in case of 3NZ-CN these values are 39.38% and 52.79%, respectively. A small amount of chlorine is also observed in both 4NZ-CN (0.31%) and 3NZ-CN (2.01%), respectively, which could be assigned to residual chlorine remaining unsubstituted after the reaction. In case of 3NZ-CN, an infinitesimally small amount of K (0.07%) was detected, attributed to K<sub>2</sub>CO<sub>3</sub> used in its synthesis. The N/C ratio for 4NZ-CN was 1.45 indicating C<sub>3</sub>N<sub>4.36</sub> as its empirical formula, while for 3NZ-CN, N/C ratio was 1.34, indicating C<sub>3</sub>N<sub>4.02</sub> as its empirical formula. The N/C ratio for g-C<sub>3</sub>N<sub>4</sub> is 1.22, which corresponds to C<sub>3</sub>N<sub>3.66</sub>. The lower N/C ratio of g-C<sub>3</sub>N<sub>4</sub> than 4NZ-CN and 3NZ-CN, indicates 4NZ-CN and 3NZ-CN have relatively higher N content.

Fig. 3g, h represents the high-resolution C-1s XPS spectra of 4NZ-CN and 3NZ-CN. For the 4NZ-CN sample, the C-1s region was deconvoluted into three peaks at binding energies of 288.1, 286.7 and 284.8 eV. The peak at 288.1 eV is assigned to N=C=N bonds in heterocyclic rings. The presence of a less intense signal at 286.7 eV may originate from C=N bonds, whereas the 284.8 eV peak can be ascribed to adventitious carbons connected through C—C bonds [42,43]. The C-1s region in 3NZ-CN was deconvoluted into three peaks, localized at 288.1, 286.5 and 284.8 eV, and assigned to N=C=N, C=N and adventitious carbons, respectively. For the 4NZ-CN sample, the N-1s region (Fig. 3j) was deconvoluted in four peaks. The highest binding energy peak at 402.1 eV was assigned to bridging N (nitrogen bonded to three carbons i.e. N-C<sub>3</sub>) and the peak at 401.3 eV could be assigned C-NH bond of tetrazole ring (pyrrolic N) and residual -NH [42,53,59]. Two intense peaks at 400.4 and 399.2 eV could be assigned to N—N and C-N=C bonds, respectively [53,60]. The presence of N—N and pyrrolic bonds reflects the presence of a tetrazole ring in 4NZ-CN structure. The presence of C-N=C bonds depicts the presence of triazine ring in 4NZ-CN structure.

In the N-1s region of 3NZ-CN (Fig. 3k) three peaks were observed at 401.3, 400.6 and 399.2 eV, corresponding to C-NH, N—N, and C-N=C bonds, respectively. In contrast to 4NZ-CN, the signal related to the N-C<sub>3</sub> feature is not present in 3NZ-CN. These observations help in predicting the structure of 4NZ-CN and 3NZ-CN. The presence of this peak in 4NZ-CN points out at the fact that there is further polymerization from bridging N, whereas the absence of this peak in 3NZ-CN indicates that the polymerization occurs on free -NH<sub>2</sub> group and not from the bridging nitrogen of 3NZ. This observation further supports the results coming from the CP.MAS measurements discussed previously. The N—N bonds and pyrrolic N in these compounds vindicates the presence of tetrazole and triazole rings in 4NZ-CN and 3NZ-CN, respectively. Furthermore, the content of N—N bond (19.69%) in 4NZ-CN is higher than that of 3NZ-CN (3.89%), which is attributed to higher N—N bond in 4NZ-CN. The Cl-2p region in 4NZ-CN and 3NZ-CN (Fig. 3i, l) was deconvoluted into four peaks centered at 202.2, 200.5, 198.9, 196.8 eV and 202.5, 200.8, 198.5, 197.3 eV, respectively. The first two peaks in both samples are assigned to C-Cl bond, whereas the latter two are probably related to ionic chlorine species [61,62].

### 3.3. Surface property studies

The N<sub>2</sub> physisorption studies were carried out to determine the textural properties of 4NZ-CN and 3NZ-CN. In particular, N<sub>2</sub> adsorption–desorption isotherms and pore size distribution plots (Fig. S13a–d) for both the samples obey Type-II physisorption and have H3 hysteresis loop, indicating their mesoporous nature. The obtained Brunauer–Emmett–Teller (BET) surface areas (S<sub>BET</sub>), pore volume, and pore diameter values for 4NZ-CN are found to be 55.80 m<sup>2</sup> g<sup>-1</sup>, 0.33 cm<sup>3</sup> g<sup>-1</sup> and 3.12 nm, respectively, whereas the corresponding values for 3NZ-CN are 52.00 m<sup>2</sup> g<sup>-1</sup>, 0.29 cm<sup>3</sup> g<sup>-1</sup> and 3.69 nm, respectively. The S<sub>BET</sub> values for both the 4NZ-CN and 3NZ-CN are higher than g-C<sub>3</sub>N<sub>4</sub> (9.20 m<sup>2</sup> g<sup>-1</sup>), indicating that these materials have a higher number of catalytically active sites. Furthermore, the number of basic sites in g-C<sub>3</sub>N<sub>4</sub>, 4NZ-CN and 3NZ-CN were ascertained using temperature programmed desorption (TPD) and results are shown in Table 1. Its values for g-C<sub>3</sub>N<sub>4</sub>, 4NZ-CN and 3NZ-CN are 0.62, 10.05 and 5.65 mmol g<sup>-1</sup>, respectively. Hence, the higher fraction of basic sites in 4NZ-CN indicates that these materials have preferential basic properties and can be better suited for CO<sub>2</sub> conversion reaction, as basic sites better activates CO<sub>2</sub> [12]. The CO<sub>2</sub>-TPD plots (Fig. S14) for 4NZ-CN and 3NZ-CN confirm this result, exhibiting two peak maxima assigned to weak and strong basic sites, with slightly higher intensity in the case of 4NZ-CN.

### 3.4. Catalytic activity studies

Firstly, the catalytic activity of 4NZ-CN was assessed for CO<sub>2</sub> cycloaddition to epoxides under solvent free conditions. The product formation was analyzed using <sup>1</sup>H NMR and <sup>13</sup>C NMR spectroscopy, as shown in sections S4 and S5. In all cases, the reaction showed 100% selectivity, as only one product, i.e., cyclic carbonate, is formed. It has to be noted, as well, that the yields reported in this paper are isolated, i.e., obtained after product purification. To find the optimal working conditions, various reaction parameters, including catalyst amount, temperature and time, were evaluated. The optimizations were done using epichlorohydrin as model substrate and the results are depicted in Fig. 4. Fig. 4a shows the catalyst amount optimization and it can be observed that the yield increases as the 4NZ-CN amount was increased from 20–50 mg. However, after 30 mg of 4NZ-CN a plateau is reached. Hence, a catalyst amount of 30 mg was chosen as optimum for further tests. Fig. 4b represents the temperature screening, and it was observed that the yield increases with the temperature. In this case, 100 °C was chosen as the best temperature. In a similar manner, the product yield increases with longer reaction times (Fig. 4c), and we selected a reaction time of 24 h for follow-up studies. Under the above-mentioned optimized conditions, the maximal yield was 60% using 30 mg of 4NZ-CN at 100 °C for 24 h. Furthermore, the yield increased to 75% when KI (20 mg) was used as a cocatalyst along with 4NZ-CN. The increase in yield is due to more readily ring opening of epoxides by KI. It can be postulated that the epoxide ring opening step is rate determining step in CO<sub>2</sub> cycloaddition to epoxides [63]. So, the iodide anion of KI attacks on less hindered carbon of epoxide and helps in the ring opening of epoxides [12]. This will further enhance the catalytic conversion of this reaction. Control experiments are shown in Fig. 4d. It was observed that there was almost undetectable product formation in the absence of catalyst, revealing that the reaction is catalytic. In case of g-C<sub>3</sub>N<sub>4</sub>, yield was 24%, under the

**Table 1**  
S<sub>BET</sub>, pore volume, pore diameter values and basic sites in 4NZ-CN and 3NZ-CN.

Sl. No.	Catalyst	S <sub>BET</sub> (m <sup>2</sup> g <sup>-1</sup> )	Pore volume (cm <sup>3</sup> g <sup>-1</sup> )	Pore Diameter (nm)	No. of basic sites (mmol g <sup>-1</sup> )
1	g-C <sub>3</sub> N <sub>4</sub>	9.20	0.21	3.70	0.62
2	4NZ-CN	55.80	0.33	3.12	10.05
3	3NZ-CN	52.00	0.29	3.69	5.65

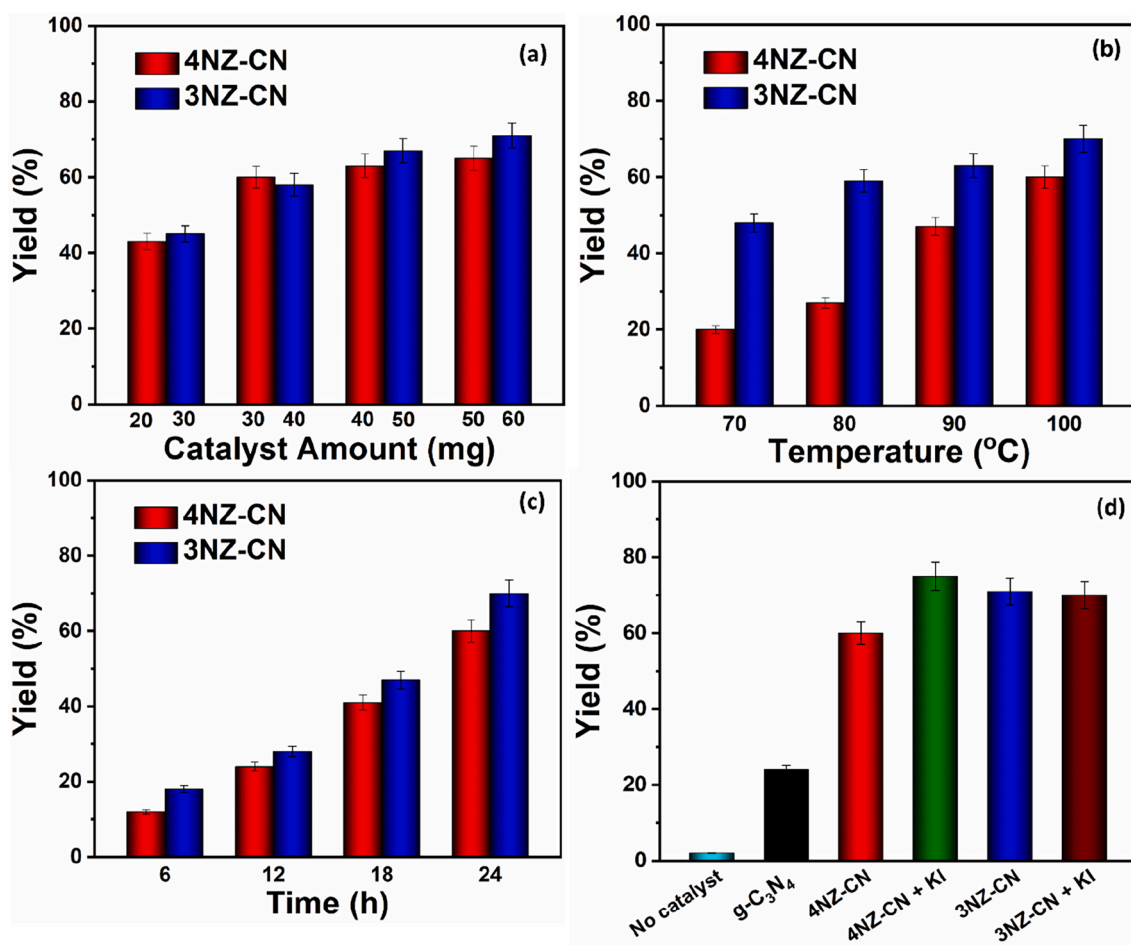


Fig. 4. Optimization of various reaction parameters for CO<sub>2</sub> cycloaddition to epichlorohydrin. (a) Catalyst amount optimization (reaction conditions: epichlorohydrin = 20 mmol, 1 atm of CO<sub>2</sub>, 100 °C, for 24 h), (b) temperature optimization (reaction conditions: epichlorohydrin = 20 mmol, 1 atm of CO<sub>2</sub>, for 24 h), (c) time optimization (reaction conditions: epichlorohydrin = 20 mmol, 1 atm of CO<sub>2</sub>) and (d) control reactions (reaction conditions: epichlorohydrin = 20 mmol, KI = 20 mg, 1 atm of CO<sub>2</sub>, for 24 h. Catalytic amount of 4NZ-CN and 3NZ-CN, used in the optimization of temperature and time was 30 and 50 mg, respectively.

conditions identified above. However, there is a significant increase in product yield (60%) when 4NZ-CN was used to catalyze this reaction. This shows the superior performance of 4NZ-CN as compared to g-C<sub>3</sub>N<sub>4</sub>, which could be attributed to a abundant number of basic sites as well as higher surface area of 4NZ-CN. The versatility of 4NZ-CN was demonstrated for different epoxides under the chosen best conditions and the substrate scope is presented in Table 2.

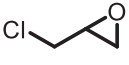
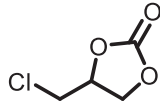
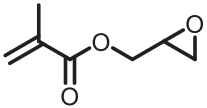
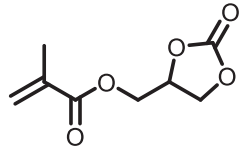
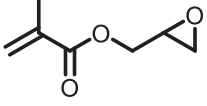
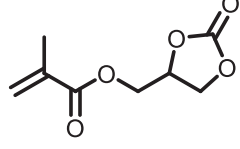
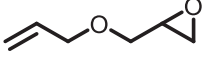
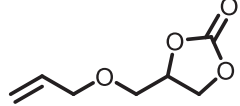
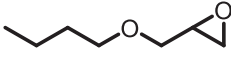
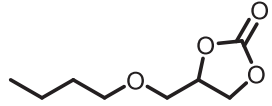
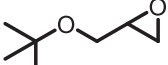
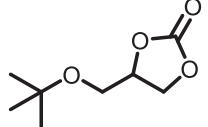
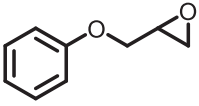
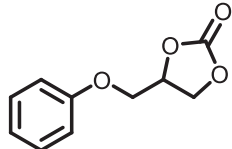
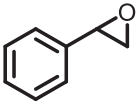
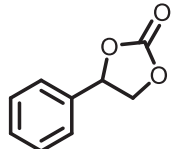
Initially, when the above-mentioned best reaction conditions were used for evaluating the substrate scope, it was observed that the product yields were relatively low. However, when the substrate amount was reduced to 10 mmol the product yield increased substantially (entries 2 and 3). For example, when 20 mmol of glycidyl methacrylate epoxide (entry 2) was used, the product yield was only 50%, whereas the yield increased to 90% when 10 mmol of glycidyl methacrylate epoxide was used (entry 3). Subsequently, 10 mmol of reactant was used for other substrates and the catalyst, 4NZ-CN showed good to very good activity for all the examined reactants. The high yield (90%) in case of glycidyl methacrylate epoxide (entry 3), is attributed to presence of greater number of oxygen atoms fascinating strong binding to catalyst surface due to hydrogen bonding [12]. In contrast, lower yield observed in case of styrene oxide is due to steric hindrance of bulky phenyl ring [64].

On the other hand, the catalytic activity of 3NZ-CN was also assessed for CO<sub>2</sub> cycloaddition to epichlorohydrin. Fig. 4a-d depicts the optimization of various reaction parameters, such as catalyst amount, temperature and time along with control reactions. The best set of conditions obtained for 3NZ-CN were determined to be 50 mg of 3NZ-

CN, 20 mg of KI and 100 °C temperature for the CO<sub>2</sub> cycloaddition to 20 mmol of epichlorohydrin, which gave 70% product yield after 24 h. Control reactions were also performed (Fig. 4d) to examine the active role of 3NZ-CN in catalyzing this reaction, which clearly demonstrates its predominant role. Negligible product formation was observed in the absence of catalyst. In addition, the product yield in case g-C<sub>3</sub>N<sub>4</sub> was also evaluated and found to be very low, indicating their inefficacy in facilitating this reaction. In the presence of 3NZ-CN the yield increased to 60%, revealing its remarkable high activity. Interestingly, it was observed that when KI was added, there is no increase in the product yield. The yield remained a little lower than 3NZ-CN alone. This could be attributed to the tethering of some potassium ions from K<sub>2</sub>CO<sub>3</sub> used in the synthesis of 3NZ-CN. In epichlorohydrin, Cl strongly binds strongly to catalyst through potassium, hindering the desorption of the product from catalyst surface, hence decreasing the product yield. The proof-of-concept for this interesting observation was verified when we explored the combination of 3NZ-CN and KI for other substrates. For other substrates, KI worked synergistically with 3NZ-CN in enhancing the yield of products. The catalytic activity of 3NZ-CN for different reactants is also presented in Table 2. The catalytic activity of 3NZ-CN was tested for glycidyl methacrylate epoxide, starting with 20 mmol, which resulted in 47% yield. When the glycidyl methacrylate amount was decreased to 10 mmol, yield increased to 88%. Subsequently, 10 mmol of reactant was used for the rest of all reactants in the substrate scope studies. Similar to its counterpart, 3NZ-CN also showed very good activity, giving good to excellent product yields. A Comparison table is constructed (Table S2),



**Table 2**  
Catalytic activity of 3NZ-CN and 3NZ-CN for different reactants.

Sl. No.	Reactant	Product	Yield (%) using 4NZ-CN as catalyst	Yield (%) using 3NZ-CN as catalyst
1 <sup>a</sup>	 <b>1a</b>	 <b>3a</b>	75	70
2 <sup>a</sup>	 <b>1b</b>	 <b>3b</b>	50	47
3 <sup>b</sup>	 <b>1c</b>	 <b>3c</b>	90	88
4 <sup>b</sup>	 <b>1d</b>	 <b>3d</b>	80	86
5 <sup>b</sup>	 <b>1e</b>	 <b>3e</b>	57	41
6 <sup>b</sup>	 <b>1f</b>	 <b>3f</b>	63	49
7 <sup>b</sup>	 <b>1g</b>	 <b>3g</b>	68	52
8 <sup>b</sup>	 <b>1h</b>	 <b>3h</b>	37	37

<sup>a</sup> Reaction conditions: epoxide = 20 mmol, catalyst (4NZ-CN = 30 mg or 3NZ-CN = 50 mg), KI = 20 mg, 1 atm CO<sub>2</sub>, 100 °C, 24 h.

<sup>b</sup> Reaction conditions: epoxide = 10 mmol, catalyst (4NZ-CN = 30 mg or 3NZ-CN = 50 mg), KI = 20 mg, 1 atm CO<sub>2</sub>, 100 °C, 24 h.

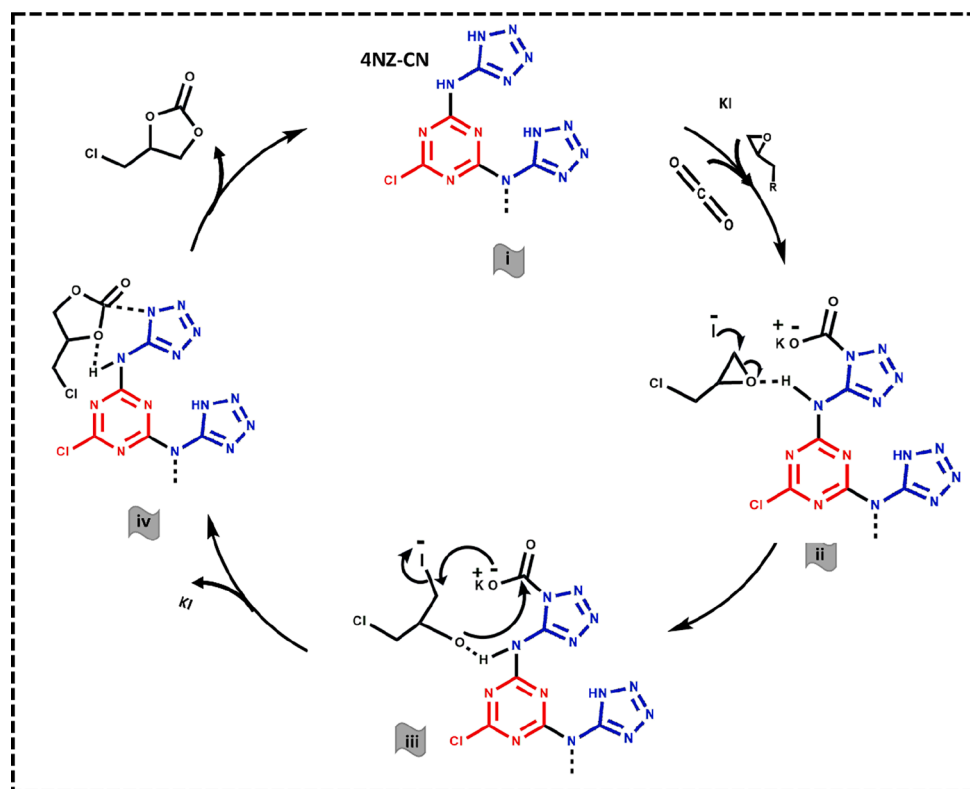
depicting the comparison of our catalysts with other carbon nitride based catalysts. Our catalysts have performed better, either in terms of mild reaction conditions, catalytic activity, amount of catalyst used or type and amount of cocatalyst used.

### 3.5. Mechanistic studies

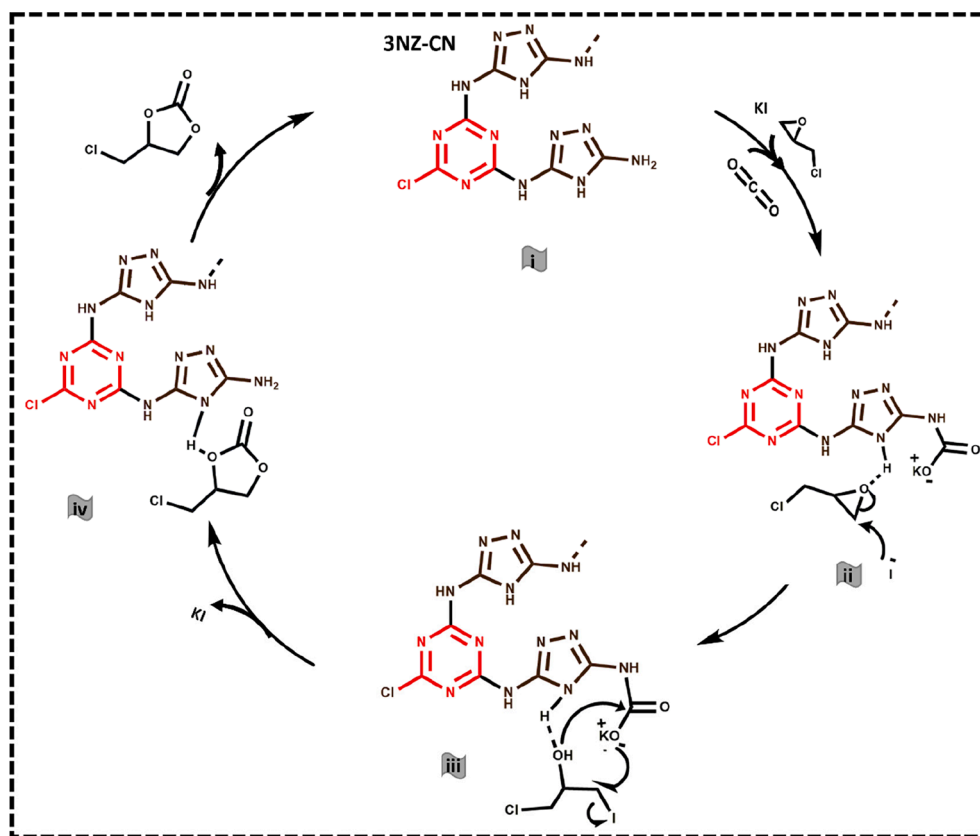
The proposed mechanisms for the cycloaddition reaction, catalyzed by 4NZ-CN and 3NZ-CN is shown in Schemes 3 and 4, respectively. Further, DFT calculations and activation parameter studies were also performed to support the proposed mechanism. As per the literature reports [65], the overall pathway for CO<sub>2</sub> cycloaddition to epoxides can be divided into three parts, epoxides ring opening, CO<sub>2</sub> insertion into the opened ring, and ring closing to liberate the cyclic carbonate, which aligns with our observations [16,65]. The mechanism was proposed by taking epichlorohydrin epoxide as a reactant. The proposed structure of 4NZ-CN is shown as (i) in Scheme 3. The reaction involves the adsorption and cooperative activation of both CO<sub>2</sub> and the epoxide by 4NZ-CN in the initial step. The nitrogen atom of the tetrazole ring attacks the carbon center of CO<sub>2</sub>, forming a carboxylate anion (intermediate ii). Simultaneously, the epoxide molecules are bonded through a hydrogen atom of the bridged –NH group, which is attacked by an iodide ion at the unsubstituted carbon of the epoxide, resulting in the opening of the epoxide ring (intermediate iii). The epoxide ring opening is considered as the rate determining step, as this step has the highest energy barrier value, as determined from kinetics and activation parameters studies. This observation has also been supported by DFT calculations. In the final step, ring closure occurs, wherein the oxide anion of the epoxide attacks the carbon center of carboxylate ion, while the oxide anion of carboxylate ion attacks the iodine-bonded carbon of the epoxide, generating the cyclic carbonate product (intermediate iv). The cyclic carbonate then desorbs from the catalyst surface and regenerates the catalyst, which will again participate in a new cycle. In Scheme 4, the proposed structure of 3NZ-CN is shown as (i).

The mechanism in this reaction is quite similar to the previous one, with the only difference being the binding of CO<sub>2</sub> and the epoxide to 3NZ-CN. In this case, the CO<sub>2</sub> molecule is attacked by the nitrogen atom of the free (unpolymerized) –NH<sub>2</sub> group rather than the N of –NH group of the triazole. This attack results in the formation of a carboxylate anion (intermediate ii). The epoxide is bonded to the hydrogen atom of the ring nitrogen and is subsequently attacked by an iodide ion, leading to the opening of the epoxide ring (intermediate iii). Here again, the epoxide ring opening step is considered as the rate determining step, which is supported by DFT and kinetics studies. In the final step, ring closure occurs, generating the cyclic carbonate product (intermediate iv), which absorbs the catalyst surface. Subsequently, the regenerated catalyst reenters the next cycle. Kinetic and thermodynamic parameter studies were conducted to investigate the reaction dynamics and gain mechanistic insights into the reaction. In particular, the reaction kinetics of CO<sub>2</sub> cycloaddition to epichlorohydrin, catalyzed by 4NZ-CN and 3NZ-CN, was evaluated by performing reactions at temperatures of 60, 80 and 100 °C, and monitoring the reaction progress at different time intervals (details are provided in S3). The semi-logarithmic plots of the epichlorohydrin concentration [A<sub>t</sub>/A<sub>0</sub>] vs time (t) (Fig. S15a, b) indicate that the reaction follows first-order kinetics when catalyzed by either 4NZ-CN or 3NZ-CN. This is expected since an excess amount of CO<sub>2</sub> was used, and its concentration will not affect the kinetics of the reaction significantly.

Furthermore, there is no change in catalyst and cocatalyst amount during the reaction, their concentrations can be considered constant. Therefore, the reaction rate depends solely on epichlorohydrin concentration. The observed rate constant values for 4NZ-CN and 3NZ-CN were determined as 2.71 × 10<sup>-5</sup> and 2.03 × 10<sup>-5</sup> s<sup>-1</sup>, respectively, at 100 °C, indicating faster reaction rate for 4NZ-CN compared to 3NZ-CN. Further, activation energy values were calculated using the Arrhenius equation and corresponding plots are provided in Fig. S15c, d. The calculated activation energy (E<sub>a</sub>) values for 4NZ-CN and 3NZ-CN, in CO<sub>2</sub> cycloaddition to epichlorohydrin were determined as 31.4 and 23.2 KJ



Scheme 3. Proposed mechanism of cycloaddition reaction catalyzed by 4NZ-CN.



Scheme 4. Proposed mechanism of cycloaddition reaction catalyzed by 3NZ-CN.

$\text{mol}^{-1}$ , respectively. Thermodynamic activation parameters, such as  $\Delta H^\ddagger$ ,  $\Delta S^\ddagger$  and  $\Delta G^\ddagger$  were determined (Table 3) from Eyring plots (Fig. S15e, f) to understand the nature of reaction [66]. The  $\Delta H^\ddagger$  and  $\Delta G^\ddagger$  values for 4NZ-CN and 3NZ-CN were 20.2, 28.5  $\text{kJ mol}^{-1}$  and 124.5, 125.4  $\text{kJ mol}^{-1}$ , respectively. The positive values of  $\Delta H^\ddagger$  and  $\Delta G^\ddagger$  vindicate the endergonic and kinetically controlled nature of this cycloaddition reaction. Additionally, the highly negative values of  $\Delta S^\ddagger$  indicates the formation of a well-organized activated complex at the transition state, consistent with previous literature [67,68]. The obtained kinetic and thermodynamic values align well with those reported in literature [66,68].

DFT calculations were conducted to investigate the mechanistic insights of proposed reaction mechanism. The modeled geometries of selected intermediates, using ECH as a reactant are shown in Fig. 5. Fig. 5a, b shows the change in Gibbs free energy ( $\Delta G$ ) for the adsorption and dissociation of molecules over 4NZ-CN and 3NZ-CN catalysts, respectively. The Gibbs free energy of  $g\text{-C}_3\text{N}_4$ , was also calculated and compared with 4NZ-CN and 3NZ-CN (Fig. S16). It was observed that Gibbs free energy values for 4NZ-CN and 3NZ-CN are lower than  $g\text{-C}_3\text{N}_4$ , indicating that 4NZ-CN and 3NZ-CN are more favored over  $g\text{-C}_3\text{N}_4$ . The change in free energy ( $\Delta G$ ) for various reaction steps was calculated according to the following equations [32]:

$$\Delta G_1 = G_{(ii)} + G_{\frac{1}{2}H_2} - (G_{(i)} + G_{CO_2} + G_{ECH} + G_{KI})$$

Table 3

$E_a$ ,  $\Delta H^\ddagger$ ,  $\Delta S^\ddagger$  and  $\Delta G^\ddagger$  values for  $CO_2$  cycloaddition to epichlorohydrin catalyzed by 4NZ-CN and 3NZ-CN.

Catalyst	$E_a$ ( $\text{kJ mol}^{-1}$ )	$\Delta H^\ddagger$ ( $\text{kJ mol}^{-1}$ )	$\Delta S^\ddagger$ ( $\text{J mol}^{-1} \text{K}^{-1}$ )	$\Delta G^\ddagger$ ( $\text{kJ mol}^{-1}$ )
4NZ-CN	31.48	28.56	-257.40	124.57
3NZ-CN	23.21	20.27	-282.00	125.46

$$\Delta G_2 = G_{(iii)} - G_{(ii)}$$

$$\Delta G_3 = G_{(iv)} + G_{KI} - G_{(iii)}$$

$$\Delta G_4 = G_{(i)} + G_{Cycliccarbonate} - G_{(iv)}$$

where  $G_{(i)}$ ,  $G_{(ii)}$ ,  $G_{(iii)}$  and  $G_{(iv)}$  represent the total energies of the (i), (ii), (iii) and (iv) intermediates as mentioned in Scheme 3 and 4.

$G_{KI}$ ,  $G_{CO_2}$ ,  $G_{ECH}$ ,  $G_{Cycliccarbonate}$  and  $G_{\frac{1}{2}H_2}$  are the total energies of KI,

$CO_2$ , epoxide, cyclic carbonate and  $H_2$ , respectively.  $\Delta G$  is negative for all the steps, indicating that these systems are thermodynamically stable. The adsorption energies of epichlorohydrin and  $CO_2$  in the simulated 4NZ-CN and 3NZ-CN structures are -1.47 and -1.07 eV, respectively. The adsorption energy value is lower for 4NZ-CN structure.

Further, the minimum energy path and activation barriers were calculated for the different steps using the climbing image nudge elastic band (CI-NEB) method (Fig. 5c, d). In the first step, which involves the adsorption of  $CO_2$  and epichlorohydrin, generating the intermediate (i) the energy barrier values for this step were determined to be 14.47  $\text{kJ mol}^{-1}$  (0.16 eV) for 4NZ-CN, and 9.64  $\text{kJ mol}^{-1}$  (0.11 eV) for 3NZ-CN. In the second step, which involves the epichlorohydrin ring opening to generate intermediate (ii), has highest energy barrier value for both the catalysts, and contributes towards the activation energy of reaction. The activation energy barrier values for 4NZ-CN and 3NZ-CN were calculated to be 27.98  $\text{kJ mol}^{-1}$  (0.29 eV) and 20.26  $\text{kJ mol}^{-1}$  (0.21 eV), respectively. These values are in good agreement with the experimentally calculated values, i.e., 31.48 and 23.21  $\text{kJ mol}^{-1}$ , respectively, determined by using Arrhenius plots. Since epichlorohydrin ring opening has the highest activation energy barrier value, this step is considered as the rate determining step, supporting the proposed mechanism. Further, step three involves the desorption of cyclic carbonate from the catalyst surface, accompanied by a decrease in activation energy barrier.

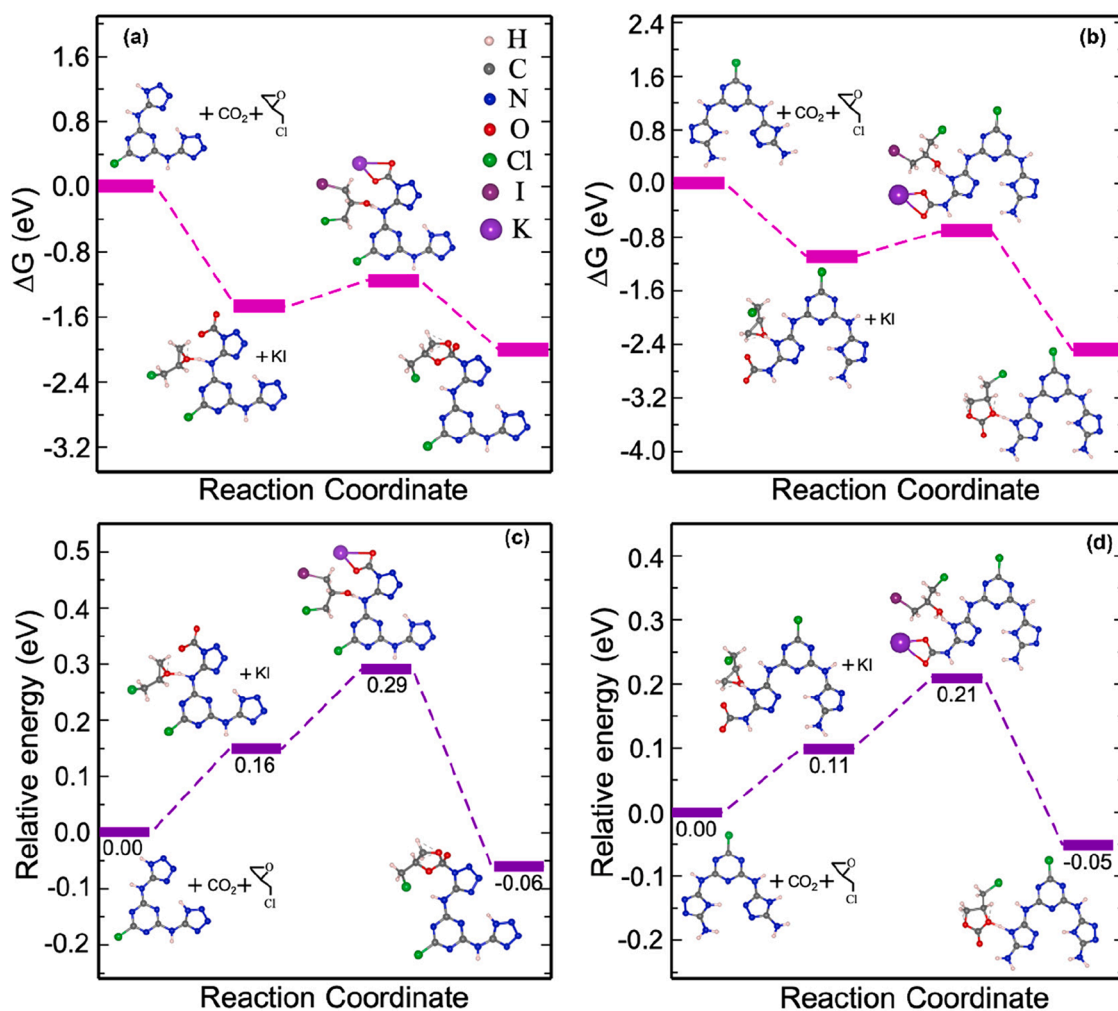


Fig. 5. Free energy profiles for the adsorption and dissociation of molecules over (a) 4NZ-CN and (b) 3NZ-CN catalysts, respectively. The minimum energy path from climbing-image NEB calculation shows the activation barrier for (c) 4NZ-CN and (d) 3NZ-CN catalysts, respectively.

### 3.6. Recyclability and stability studies

The recyclability tests were performed for both 4NZ-CN and 3NZ-CN catalysts, and results were shown in Fig. S17. The experiments were conducted with epichlorohydrin under the chosen best conditions. After each cycle, the catalysts were recovered from the reaction mixture by centrifugation, followed by multiple washings of ethyl acetate and ethanol multiple times, and dried at 80 °C for 12 h. Fig. S17a depicts the recyclability plots for 4NZ-CN and 3NZ-CN catalysts under the chosen best conditions. In addition, the FTIR spectra of 4NZ-CN and 3NZ-CN recovered after four cycles is shown in Fig. S17b, c. It can be evidenced that in contrast to its counterpart, 3NZ-CN showed promising performance up to four cycles without any significant loss in activity revealing better reusability of 3NZ-CN catalyst for this reaction.

## 4. Conclusions

In this work, we have prepared two novel catalysts, 4NZ-CN and 3NZ-CN, using a facile, energy-efficient, and economically favorable synthesis route. XRD analyses indicate the effective polymerization of the 4NZ and 3NZ precursors into novel CN. CPMAS NMR, FTIR, Raman, and XPS studies revealed the presence of triazine and tetrazole moieties in 4NZ-CN, and triazine and triazole moieties in 3NZ-CN. Both 4NZ-CN and 3NZ-CN exhibit high surface areas (55.8 and 52.0 m<sup>2</sup> g<sup>-1</sup>) and abundant basic sites compared to conventional g-C<sub>3</sub>N<sub>4</sub>, which directly contributes to their excellent catalytic activity for CO<sub>2</sub> cycloaddition to

epichlorohydrin. Furthermore, both catalysts showed good to excellent product yields for various reactant substrates, showcasing their wide applicability. The microkinetic analysis, have shown a high positive value of  $\Delta H^\ddagger$  (28.56 and 20.27 kJ mol<sup>-1</sup>) and  $\Delta G^\ddagger$  (124.57 and 125.46 kJ mol<sup>-1</sup>), and negative value of activation entropy  $\Delta S^\ddagger$  (-257.40 and 282.00 J mol<sup>-1</sup>) for 4NZ-CN and 3NZ-CN, respectively, indicating that the reaction is endergonic and kinetically controlled. DFT and thermodynamic activation parameter studies revealed that the epoxide ring opening is the rate-determining step for this cycloaddition reaction, which is key to control the product selectivity. Detailed kinetic and computational studies were performed to understand the catalytic mechanism involved in this reaction. This work opens new avenues for the exploration of facile, scalable, energy-efficient, and economically favorable approaches for the synthesis of carbon nitrides, which can be readily employed not only for CO<sub>2</sub> conversion but also for several other industrially relevant catalytic reactions.

### CRedit authorship contribution statement

**Hushan Chand:** Writing – review & editing, Writing – original draft, Visualization, Validation, Software, Project administration, Methodology, Investigation, Formal analysis, Data curation, Conceptualization. **Preeti Bhumla:** Writing – review & editing, Methodology, Formal analysis. **Subhadip Goswami:** Writing – review & editing, Methodology, Formal analysis. **Nicolo Allasia:** Writing – review & editing, Methodology, Formal analysis. **Gianvito Vilé:** Writing – review &

editing, Supervision, Methodology, Funding acquisition. **Saswata Bhattacharya**: Writing – review & editing, Supervision, Methodology, Funding acquisition. **Venkata Krishnan**: Writing – review & editing, Supervision, Resources, Methodology, Funding acquisition, Conceptualization.

### Declaration of competing interest

The authors declare that they have no known competing financial interests or personal relationships that could have appeared to influence the work reported in this paper.

### Data availability

Data will be made available on request.

### Acknowledgments

Advanced Materials Research Centre (AMRC), Indian Institute of Technology Mandi is gratefully acknowledged for providing all the necessary characterization facilities. HC thanks the Ministry of Education (MoE), Government of India for the doctoral fellowship. PB acknowledges University Grants Commission (UGC), India, for the senior research fellowship [1392/(CSIR-UGC NET JUNE 2018)].

### Appendix A. Supplementary material

Supplementary data to this article can be found online at <https://doi.org/10.1016/j.jcis.2024.06.031>.

### References

- S. Singh, R. Verma, N. Kaul, J. Sa, A. Punjal, S. Prabhu, V. Polshettiwar, Surface plasmon-enhanced photo-driven CO<sub>2</sub> hydrogenation by hydroxy-terminated nickel nitride nanosheets, *Nat. Commun.* 14 (1) (2023) 2551.
- H. Chand, A. Kumar, V. Krishnan, Borophene and boron-based nanosheets: recent advances in synthesis strategies and applications in the field of environment and energy, *Adv. Mater. Interfaces* 8 (15) (2021) 2100045.
- S. Bhattacharjee, M. Rahaman, V. Andrei, M. Miller, S. Rodríguez-Jiménez, E. Lam, C. Pornrungraj, E. Reisner, Photoelectrochemical CO<sub>2</sub>-to-fuel conversion with simultaneous plastic reforming, *Nat. Synth.* 2 (2023) 1–11.
- S.N. Talapaneni, G. Singh, I.Y. Kim, K. AlBahily, A.a.H. Al-Muhtaseb, A.S. Karakoti, E. Tavakkoli, A. Vinu, Nanostructured carbon nitrides for CO<sub>2</sub> capture and conversion, *Adv. Mater.* 32(18) (2020) 1904635.
- Y. Xu, Y. Ren, G. Zhou, S. Feng, Z. Yang, S. Dai, Z. Lu, T. Zhou, Amide-engineered metal-organic porous liquids toward enhanced CO<sub>2</sub> photoreduction performance, *Adv. Funct. Mater.* 34 (2024) 2313695.
- G. Zhou, Y. Xu, Y. Cheng, Z. Yu, B. Wei, X. Liu, Z. Chen, C. Li, Z. Lu, Rapid dissociation of high concentration excitons between [Bi<sub>2</sub>O<sub>2</sub>]<sup>2+</sup> slabs with multifunctional N-Bi-O sites for selective photoconversion into CO, *Appl. Catal. b: Environ.* 335 (2023) 122892.
- A. Centeno-Pedraza, J. Perez-Arce, Z. Freixa, P. Ortiz, E.J. Garcia-Suarez, Catalytic systems for the effective fixation of CO<sub>2</sub> into epoxidized vegetable oils and derivatives to obtain biobased cyclic carbonates as precursors for greener polymers, *Ind. Eng. Chem. Res.* 62 (8) (2023) 3428–3443.
- A. Eskemeh, H. Chand, A. Karmakar, V. Krishnan, R.R. Koner, Zn-MOF as a single catalyst with dual Lewis acidic and basic reaction sites for CO<sub>2</sub> fixation, *Inorg. Chem.* 63 (8) (2024) 3757–3768.
- G. Li, S. Dong, P. Fu, Q. Yue, Y. Zhou, J. Wang, Synthesis of porous poly (ionic liquid) s for chemical CO<sub>2</sub> fixation with epoxides, *Green Chem.* 24 (9) (2022) 3433–3460.
- S.N. Talapaneni, G. Singh, I.Y. Kim, K. AlBahily, A.a.H. Al-Muhtaseb, A.S. Karakoti, E. Tavakkoli, A. Vinu, Nanostructured Carbon Nitrides for CO<sub>2</sub> Capture and Conversion, *Adv. Mater.* 32(18) (2020) 1904635.
- H. Chand, A. Kumar, S. Goswami, V. Krishnan, Comparison of catalytic activity of graphitic carbon nitrides derived from different precursors for carbon dioxide conversion, *Fuel* 357 (2024) 129757.
- H. Chand, P. Choudhary, A. Kumar, A. Kumar, V. Krishnan, Atmospheric pressure conversion of carbon dioxide to cyclic carbonates using a metal-free Lewis acid-base bifunctional heterogeneous catalyst, *J. CO<sub>2</sub> Util.* 51 (2021) 101646.
- Z. Huang, F. Li, B. Chen, G. Yuan, Cycloaddition of CO<sub>2</sub> and epoxide catalyzed by amino- and hydroxyl-rich graphitic carbon nitride, *Cat. Sci. Technol.* 6 (9) (2016) 2942–2948.
- S. Asadzadeh-Khaneghah, A. Habibi-Yangjeh, D. Seifzadeh, H. Chand, V. Krishnan, G- G-C<sub>3</sub>N<sub>4</sub> nanosheets adhered with Ag<sub>3</sub>BiO<sub>3</sub> and carbon dots with appreciably promoted photoactivity towards elimination of several contaminants, *Adv. Powder Technol.* 32 (4) (2021) 1196–1206.
- S. Asadzadeh-Khaneghah, A. Habibi-Yangjeh, D. Seifzadeh, H. Chand, V. Krishnan, Visible-light-activated g-C<sub>3</sub>N<sub>4</sub> nanosheet/carbon dot/FeOCl nanocomposites: photodegradation of dye pollutants and tetracycline hydrochloride, *Colloids Surf. A Physicochem. Eng. Asp.* 617 (2021) 126424.
- J. Zhu, T. Diao, W. Wang, X. Xu, X. Sun, S.A. Carabineiro, Z. Zhao, Boron doped graphitic carbon nitride with acid-base duality for cycloaddition of carbon dioxide to epoxide under solvent-free condition, *Appl. Catal. B Environ.* 219 (2017) 92–100.
- O. Iqbal, H. Ali, N. Li, M.Z. Ansari, A.I. Al-Sulami, K.F. Alshammari, H.S. Abd-Rabbah, Y. Al-Hadeethi, T. Taha, A. Zada, A review on the synthesis, properties, and characterizations of graphitic carbon nitride (g-C<sub>3</sub>N<sub>4</sub>) for energy conversion and storage applications, *Mater. Today Phys.* 34 (2023) 101800.
- G. Algara-Siller, N. Severin, S.Y. Chong, T. Björkman, R.G. Palgrave, A. Laybourn, M. Antonietti, Y.Z. Khimyak, A.V. Krashennnikov, J.P. Rabe, Triazine-based graphitic carbon nitride: a two-dimensional semiconductor, *Angew. Chem. Int. Ed.* 53 (29) (2014) 7450–7455.
- J. Zhu, P. Xiao, H. Li, S.A.C. Carabineiro, Graphitic carbon nitride: synthesis, properties, and applications in catalysis, *ACS Appl. Mater. Interfaces* 6 (19) (2014) 16449–16465.
- W.K. Darkwah, Y. Ao, Mini review on the structure and properties (Photocatalysis), and preparation techniques of graphitic carbon nitride nano-based particle, and its applications, *Nanoscale Res. Lett.* 13 (1) (2018) 388.
- J. Ma, J. Das, J. Zhang, J. Cheng, S. Sorcar, B.A. Rosen, P. Shekhter, R. Dobrovetsky, E. Flaxer, Y. Yavor, Carbon-nitride popcorn—a novel catalyst prepared by self-propagating combustion of nitrogen-rich triazines, *Small* 19 (2023) 2205994.
- Z. Zhu, C. Ma, K. Yu, Z. Lu, Z. Liu, P. Huo, X. Tang, Y. Yan, Synthesis Ce-doped biomass carbon-based g-C<sub>3</sub>N<sub>4</sub> via plant growing guide and temperature-programmed technique for degrading 2-Mercaptobenzothiazole, *Appl. Catal. B: Environ.* 268 (2020) 118432.
- M.A. Bajada, G. Di Liberto, S. Tosoni, V. Ruta, L. Mino, N. Allasia, A. Sivo, G. Pacchioni, G. Vilé, Light-driven C-O coupling of carboxylic acids and alkyl halides over a Ni single-atom catalyst, *Nat. Synth.* 2 (11) (2023) 1092–1103.
- K.S. Lakhi, D.-H. Park, K. Al-Bahily, W. Cha, B. Viswanathan, J.-H. Choy, A. Vinu, Mesoporous carbon nitrides: synthesis, functionalization, and applications, *Chem. Soc. Rev.* 46 (1) (2017) 72–101.
- X. Guan, M. Fawaz, R. Sarkar, C.-H. Lin, Z. Li, Z. Lei, P.D. Nithinraj, P. Kumar, X. Zhang, J.-H. Yang, L. Hu, T. Wu, S. Chakraborty, J. Yi, A. Vinu, S-doped C<sub>3</sub>N<sub>5</sub> derived from thiazazole for efficient photocatalytic hydrogen evolution, *J. Mater. Chem. A* 11 (2023) 12837–12845.
- P. Kumar, E. Vahidzadeh, U.K. Thakur, P. Kar, K.M. Alam, A. Goswami, N. Mahdi, K. Cui, G.M. Bernard, V.K. Michaelis, C<sub>3</sub>N<sub>5</sub>: a low bandgap semiconductor containing an azo-linked carbon nitride framework for photocatalytic, photovoltaic and adsorbent applications, *J. Am. Chem. Soc.* 141 (13) (2019) 5415–5436.
- G.P. Mane, D.S. Dhawale, C. Anand, K. Ariga, Q. Ji, M.A. Wahab, T. Mori, A. Vinu, elective sensing performance of mesoporous carbon nitride with a highly ordered porous structure prepared from 3-amino-1, 2, 4-triazine, *J. Mater. Chem. A* 1 (8) (2013) 2913–2920.
- G. Kresse, J. Hafner, Ab initio molecular dynamics for liquid metals, *Phys. Rev. B* 47 (1) (1993) 558.
- G. Kresse, D. Joubert, From ultrasoft pseudopotentials to the projector augmented-wave method, *Phys. Rev. B* 59 (3) (1999) 1758.
- J.P. Perdew, K. Burke, M. Ernzerhof, Generalized gradient approximation made simple, *Phys. Rev. Lett.* 77 (18) (1996) 3865.
- A.V. Krukau, O.A. Vydrov, A.F. Izmaylov, G.E. Scuseria, Influence of the exchange screening parameter on the performance of screened hybrid functionals, *J. Chem. Phys.* 125 (22) (2006) 224106.
- P. Bhumla, M. Kumar, S. Bhattacharya, Theoretical insights into C-H bond activation of methane by transition metal clusters: the role of anharmonic effects, *Nanoscale Adv.* 3 (2) (2021) 575–583.
- G. Henkelman, H. Jónsson, Improved tangent estimate in the nudged elastic band method for finding minimum energy paths and saddle points, *J. Chem. Phys.* 113 (22) (2000) 9978–9985.
- A. Tkatchenko, M. Scheffler, Accurate molecular van der Waals interactions from ground-state electron density and free-atom reference data, *Phys. Rev. Lett.* 102 (7) (2009) 073005.
- K. Momma, F. Izumi, VESTA3 for three-dimensional visualization of crystal, volumetric and morphology data, *J. Appl. Cryst.* 44 (6) (2011) 1272–1276.
- C. Ruhlmeier, M. Taplick, M. Nissen, I. Baev, C. Strelow, S. Hentschel, M. Dohrmann, M. Martins, T. Kipp, A. Mews, Deposition of triazine-based graphitic carbon nitride via plasma-induced polymerisation of melamine, *J. Mater. Chem. A* 10 (17) (2022) 9680–9692.
- V. Mutreja, S. Singh, A. Ali, Potassium impregnated nanocrystalline mixed oxides of La and Mg as heterogeneous catalysts for transesterification, *Renew. Energy* 62 (2014) 226–233.
- X. Zhang, G. Zhou, M. Wang, X. Wang, W. Jiang, H. Zhou, Performance of gamma-Al<sub>2</sub>O<sub>3</sub> decorated with potassium salts in the removal of CS<sub>2</sub> from C<sub>5</sub> cracked distillate, *RSC Adv.* 11 (25) (2021) 15351–15359.
- D. Dontsova, S. Pronkin, M. Wehle, Z. Chen, C. Fettekenhauer, G. Clavel, M. Antonietti, Triazoles: a new class of precursors for the synthesis of negatively charged carbon nitride derivatives, *Chem. Mater.* 27 (15) (2015) 5170–5179.
- A. Savateev, S. Pronkin, J.D. Epping, M.G. Willinger, M. Antonietti, D. Dontsova, Synthesis of an electronically modified carbon nitride from a processable



- semiconductor, 3-amino-1, 2, 4-triazole oligomer, via a topotactic-like phase transition, *J. Mater. Chem. A* 5 (18) (2017) 8394–8401.
- [41] C. Yu, J. Jin, H. Yan, G. Zhou, Y. Xu, L. Tang, X. Liu, H. Li, K. Zhang, Z. Lu, Spaced double hydrogen bonding for highly efficient and selective photocatalytic air reductive  $\text{H}_2\text{O}_2$  synthesis, *Angew. Chem. Int. Ed.* 63 (2024) e202400857.
- [42] Q. Dong, N. Mohamad Latiff, V. Mazánek, N.F. Rosli, H.L. Chia, Z.k. Sofer, M. Pumera, Triazine-and Heptazine-based carbon nitrides: toxicity, *ACS Appl. Nano Mater.* 1 (9) (2018) 4442–4449.
- [43] G.P. Mane, S.N. Talapaneni, K.S. Lakhi, H. Ilbeygi, U. Ravon, K. Al-Bahily, T. Mori, D.H. Park, A. Vinu, Highly ordered nitrogen-rich mesoporous carbon nitrides and their superior performance for sensing and photocatalytic hydrogen generation, *Angew. Chem. Int. Ed.* 56 (29) (2017) 8481–8485.
- [44] S.N. Talapaneni, G.P. Mane, D.-H. Park, K.S. Lakhi, K. Ramadass, S. Joseph, W. M. Skinner, U. Ravon, K. Al-Bahily, A. Vinu, Diaminotetrazine based mesoporous  $\text{C}_3\text{N}_6$  with a well-ordered 3D cubic structure and its excellent photocatalytic performance for hydrogen evolution, *J. Mater. Chem. A* 5 (34) (2017) 18183–18192.
- [45] C. Sathish, S. Premkumar, X. Chu, X. Yu, M.B. Breese, M. Al-Abri, A.a.H. Al-Muhtaseb, A. Karakoti, J. Yi, A. Vinu, Microporous carbon nitride ( $\text{C}_3\text{N}_{5,4}$ ) with tetrazine based molecular structure for efficient adsorption of  $\text{CO}_2$  and water, *Angew. Chem., Int. Ed.* 133 (60) (2021) 21242.
- [46] M.S. Akdemir, M. Simian, P. Theato, H. Mutlu, Synthesis of novel (bis)-1,5-disubstituted-1H-tetrazole-decorated monomers and their respective polymers via thiol-ene polymerization, *Macromol. Chem. Phys.* 224 (3) (2023) 2200371.
- [47] T. Suter, V. Brázdová, K. McColl, T.S. Miller, H. Nagashima, E. Salvadori, A. Sella, C.A. Howard, C.W. Kay, F. Corà, Synthesis, structure and electronic properties of graphitic carbon nitride films, *J. Phys. Chem. C* 122 (44) (2018) 25183–25194.
- [48] Q. Dong, N. Mohamad Latiff, V. Mazánek, N.F. Rosli, H.L. Chia, Z. Sofer, M. Pumera, Triazine- and heptazine-based carbon nitrides: toxicity, *ACS Appl. Nano Mater.* 1 (9) (2018) 4442–4449.
- [49] H.L. Lee, Z. Sofer, V. Mazánek, J. Luxa, C.K. Chua, M. Pumera, Graphitic carbon nitride: effects of various precursors on the structural, morphological and electrochemical sensing properties, *Appl. Mater. Today* 8 (2017) 150–162.
- [50] T. Chhabra, A. Bahuguna, S.S. Dhankhar, C. Nagaraja, V. Krishnan, Sulfonated graphitic carbon nitride as a highly selective and efficient heterogeneous catalyst for the conversion of biomass-derived saccharides to 5-hydroxymethylfurfural in green solvents, *Green Chem.* 21 (21) (2019) 6012–6026.
- [51] A. Hammerl, M.A. Hiskey, G. Holl, T.M. Klapötke, K. Polborn, J. Stierstorfer, J. Weigand, Azidoformamidineum and guanidineum 5, 5'-azotetrazolate salts, *Chem. Mater.* 17 (14) (2005) 3784–3793.
- [52] P. Kumar, E. Vahidzadeh, U.K. Thakur, P. Kar, K.M. Alam, A. Goswami, N. Mahdi, K. Cui, G.M. Bernard, V.K. Michaelis, K. Shankar,  $\text{C}_3\text{N}_5$ : a low bandgap semiconductor containing an Azo-linked carbon nitride framework for photocatalytic, photovoltaic and adsorbent applications, *J. Am. Chem. Soc.* 141 (13) (2019) 5415–5436.
- [53] I.Y. Kim, S. Kim, S. Premkumar, J.H. Yang, S. Umaphathy, A. Vinu, Thermodynamically stable mesoporous  $\text{C}_3\text{N}_7$  and  $\text{C}_3\text{N}_6$  with ordered structure and their excellent performance for oxygen reduction reaction, *Small* 16 (12) (2020) 1903572.
- [54] Y. Liu, P. Yi, L. Gong, X. Yi, P. He, T. Wang, J. Zhang, Three-dimensional metal-organic frameworks as super heat-resistant explosives: potassium 4,4'-Oxybis[3,3'-(5-tetrazolyl)furazan and potassium (1,2,4-Triazol-3-yl)tetrazole, *Inorg. Chem.* 62 (7) (2023) 3186–3194.
- [55] D. Chand, C. He, J.P. Hooper, L.A. Mitchell, D.A. Parrish, J.N.M. Shreeve, Mono- and diiodo-1,2,3-triazoles and their mono nitro derivatives, *Dalton Trans.* 45 (23) (2016) 9684–9688.
- [56] R. Tang, J. Wen, R.E. Stote, Y. Sun, Cyanuric chloride-based reactive dyes for use in the antimicrobial treatments of polymeric materials, *ACS Appl. Mater. Interfaces* 13 (1) (2021) 1524–1534.
- [57] M. Porchia, F. Tisato, F. Refosco, C. Bolzati, M. Cavazza-Ceccato, G. Bandoli, A. Dolmella, New Approach to the Chemistry of Technetium(V) and Rhenium(V) Phenylimido Complexes: Novel  $[\text{M}(\text{NPh})\text{PNP}]^{3+}$  Metal Fragments (M = Tc, Re; PNP = Aminodiphosphine) Suitable for the Synthesis of Stable Mixed-Ligand Compounds, *Inorg. Chem.* 44 (13) (2005) 4766–4776.
- [58] S.P. Gabuda, S.G. Kozlova, N.B. Kompankov, K.S. Redkina, Effect of a two-phase boundary in  $\text{D}_2\text{O}$ /triethylamine solution: an  $^1\text{H}$  NMR study, *Fluid Phase Equilib.* 443 (2017) 9–13.
- [59] A. Samikannu, L.J. Konwar, P. Mäki-Arvela, J.-P. Mikkola, Renewable N-doped active carbons as efficient catalysts for direct synthesis of cyclic carbonates from epoxides and  $\text{CO}_2$ , *Appl. Catal. B Environ.* 241 (2019) 41–51.
- [60] I.Y. Kim, S. Kim, X. Jin, S. Premkumar, G. Chandra, N.S. Lee, G.P. Mane, S. J. Hwang, S. Umaphathy, A. Vinu, Ordered mesoporous  $\text{C}_3\text{N}_5$  with a combined triazole and triazine framework and its graphene hybrids for the oxygen reduction reaction (ORR), *Angew. Chem. Int. Ed.* 130 (57) (2018) 17135–17140.
- [61] Q. Gu, Z. Gao, C. Xue, Self-sensitized carbon nitride microspheres for long-lasting visible-light-driven hydrogen generation, *Small* 12 (26) (2016) 3543–3549.
- [62] M. Li, Q. Zheng, D.P. Durkin, H. Chen, D. Shuai, Environmental application of chlorine-doped graphitic carbon nitride: continuous solar-driven photocatalytic production of hydrogen peroxide, *J. Hazard. Mater.* 436 (2022) 129251.
- [63] A.C. Deacy, A. Phanopoulos, W. Lindeboom, A. Buchard, C.K. Williams, Insights into the mechanism of carbon dioxide and propylene oxide ring-opening copolymerization using a Co(III)/K(I) heterodinuclear catalyst, *J. Am. Chem. Soc.* 144 (39) (2022) 17929–17938.
- [64] Q. Yang, H. Peng, Q. Zhang, X. Qian, X. Chen, X. Tang, S. Dai, J. Zhao, K. Jiang, Q. Yang, Atomically dispersed high-density Al– $\text{N}_4$  sites in porous carbon for efficient photodriven  $\text{CO}_2$  cycloaddition, *Adv. Mater.* 33 (45) (2021) 2103186.
- [65] F. Della Monica, B. Maity, T. Pehl, A. Buonerba, A. De Nisi, M. Monari, A. Grassi, B. Rieger, L. Cavallo, C. Capacchione, [OSSO]-type iron (III) complexes for the low-pressure reaction of carbon dioxide with epoxides: catalytic activity, reaction kinetics, and computational study, *ACS Catal.* 8 (8) (2018) 6882–6893.
- [66] S. Das, J. Zhang, T.W. Chamberlain, G.J. Clarkson, R.I. Walton, Nonredox  $\text{CO}_2$  fixation in solvent-free conditions using a lewis acid metal-organic framework constructed from a sustainably sourced ligand, *Inorg. Chem.* 61 (46) (2022) 18536–18544.
- [67] A. Rehman, V.C. Eze, M.G. Resul, A. Harvey, Kinetics and mechanistic investigation of epoxide/ $\text{CO}_2$  cycloaddition by a synergistic catalytic effect of pyrrolidinopyridinium iodide and zinc halides, *J. Energy Chem.* 37 (2019) 35–42.
- [68] A. Rehman, F. Saleem, F. Javed, H. Qutab, V.C. Eze, A. Harvey, Kinetic study for styrene carbonate synthesis via  $\text{CO}_2$  cycloaddition to styrene oxide using silica-supported pyrrolidinopyridinium iodide catalyst, *J. CO<sub>2</sub> Util.* 43 (2021) 101379.